Available on CMS information server

CMS NOTE 2006/077

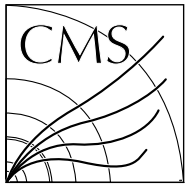

The Compact Muon Solenoid Experiment

CMS Note

Mailing address: CMS CERN, CH-1211 GENEVA 23, Switzerland

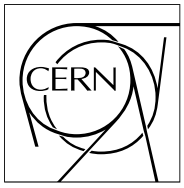

18 May 2006

Measurement of top-pair cross section and top-quark mass in the di-lepton and full-hadronic channels with CMS

Martina Davids, Markus Duda, Stefan Kasselmann, Daiske Tornier

RWTH Aachen, III Physikalisches Institut B, Physikzentrum-RWTH Aachen, D-52056 Aachen, Germany

Andrea Castro, Claudia Ciocca

Dipartimento di Fisica, Università degli Studi di Bologna, Italy

Javier Cuevas Maestro, Jesús Vizán

University of Oviedo, Spain

Fabrizio Palla, Marcel Vos

INFN Sezione di Pisa, Italy

D.Cano Fernández, I. González Caballero, R. Vilar

IFCA(CSIC-U. Cantabria) Spain

Abstract

This note describes the selection and reconstruction of top-pair events with the CMS detector at the LHC, and the determination of the top-quark mass. Two of the three main channels, classified by the decay of the W boson arising in top decay, are considered here: di-lepton and fully hadronic $t\bar{t}$ events. The performance of the selections, the resulting cross section measurements, and the mass reconstruction accuracy are evaluated based on a detailed simulation of the CMS detector.

1 Introduction

This note describes the selection and reconstruction of top-pair events with the CMS detector at the LHC, and the determination of the top-quark mass. Two of the three main channels, classified by the decay of the W boson arising in top decay, are considered here: di-lepton and fully hadronic $t\bar{t}$ events. The performance of the selections, the resulting cross section measurements, and the mass reconstruction accuracy are evaluated based on a detailed simulation of the CMS detector.

The leading-order cross section for $t\bar{t}$ production at the LHC is 488 pb, while the next-to-leading order including the resummation of Sudakov logarithms is 830 pb. Since the simulation of both signal and background event samples is to leading order, the corresponding leading-order cross sections are used throughout. Luminosities in a range of up to several tens of 1/fb are considered.

The following sections present the details on the di-lepton channel (section 2) and the fully hadronic channel (sections 3 and 4). Section 2 presents a selection and mass determination for an initial luminosity of 1/fb, as well as the selection for higher luminosities and for top decays into tau leptons. The selection of the fully hadronic channel is described in section 3, while section 4 presents the mass analysis in this channel. Summary and conclusions are given in section 5.

2 Selection of Di-Lepton Events

The di-lepton decay channel denotes the case where the two W bosons from the decaying $t\bar{t}$ pair both decay to final states containing an electron or a muon, accounting for about 5% of all $t\bar{t}$ SM decays. Measuring the rate of the reaction $t\bar{t} \to b\ell^+\nu_\ell \bar{b}\ell'^-\bar{\nu}_{\ell'}$ tests both the production and decay mechanisms of the top quark.

These events are characterised by two high-energy leptons, two jets from the hadronisation of the b quarks, and large missing energy from the two unobserved neutrinos. Additional jets are often produced by initial-state and final-state radiation.

In general, the reconstruction and selection of di-lepton $t\bar{t}$ events is based on reconstructing the directions and energies or momenta of isolated electrons, muons and jets, and on reconstructing the missing transverse energy $\not{E}_{\mathrm{T}}$ from the transverse momentum balance in the event. The purity of the event samples is enhanced by identifying jets that originated from a b quark (b tagging), since in the Standard Model every $t\bar{t}$ event contains two b jets.

2.1 Event Selection and Mass Determination for 1/fb

2.1.1 Event selection

For an integrated luminosity of $1\ \mathrm{fb}^{-1}$ about 54000 signal events are expected according to the leading-order estimate of PYTHIA. The main backgrounds with a final state mimicking the signal are Z production accompanied by jets and di-boson production with jets. Misidentified leptons and leptons from b-jets in $t\bar{t}$ events represent another important and later dominating background. Here, dilepton events with W bosons decaying into τ-leptons are considered signal events if the τ's decay leptonically.

Events are required to pass the Level-1 and High Level Trigger, in particular the single and di-lepton subtriggers. In addition to trigger criteria, events must contain at least two jets and two oppositely charged leptons. Electrons are identified using an electron likelihood method combining various electromagnetic shower variables, i.e. the energy distribution in the electromagnetic calorimeter cells and the ratio of deposited energy in the electromagnetic and hadronic calorimeter, and track-to-supercluster-matching criteria. After this preselection about 15000 signal events are left with a signal over background ratio of $S : B = 1 : 10$. The most important background at this stage consists of Z+jets production with an accepted cross section of about 120 pb and similar final state.

Further cuts are applied to specifically reduce the number of Z+jets events as well as the contribution of the other $t\bar{t}$ channels. To reduce the background from misidentified leptons and leptons in b-jets, a lepton will be rejected if it does not satisfy track or calorimeter isolation criteria. The track isolation, as illustrated in figure 1 requires no tracks with significant transverse momentum (more than 10% if the lepton p_{T}) in a $\Delta R < 0.2$ cone around the lepton candidate. The required two charged leptons are then chosen with a discriminant based on the likelihood ratio in case of an electron, the energy deposited in a cone of $\Delta R = 0.2$ around the lepton axis and the p_{T} of the lepton.

Both b-jets are selected with a discriminator based on the jet p_{T}, the invariant mass of tracks inside the jet and the btag-value [1]. Using this scheme both the jets and leptons of the signal are selected with a purity (in case there

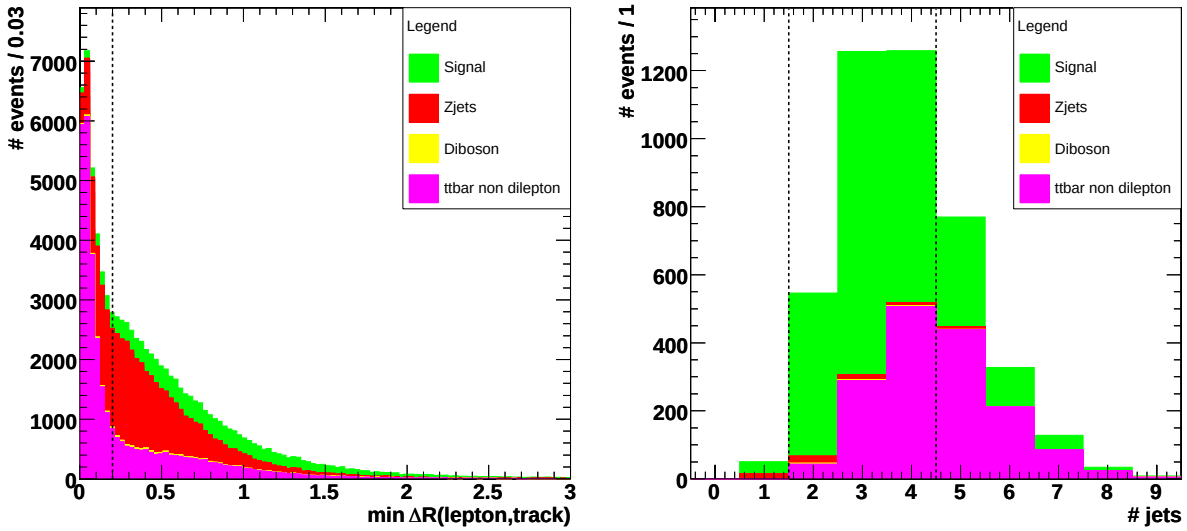

Figure 1: Left: Cut on the minimal distance in ΔR between the lepton candidate and the closest nearby track. Right: All cuts applied, except a cut on the number of jets with p_{T} greater than $30\ \mathrm{GeV}/c$. Both plots are scaled to $1\ \mathrm{fb}^{-1}$

is an object reconstructed) of more than 90%. It has been shown in reference [1] that, during the *first data taking phases* of the LHC, the degradation in b-tagging performance is still acceptable. This implies that the b-tagging results presented here remain essentially correct.

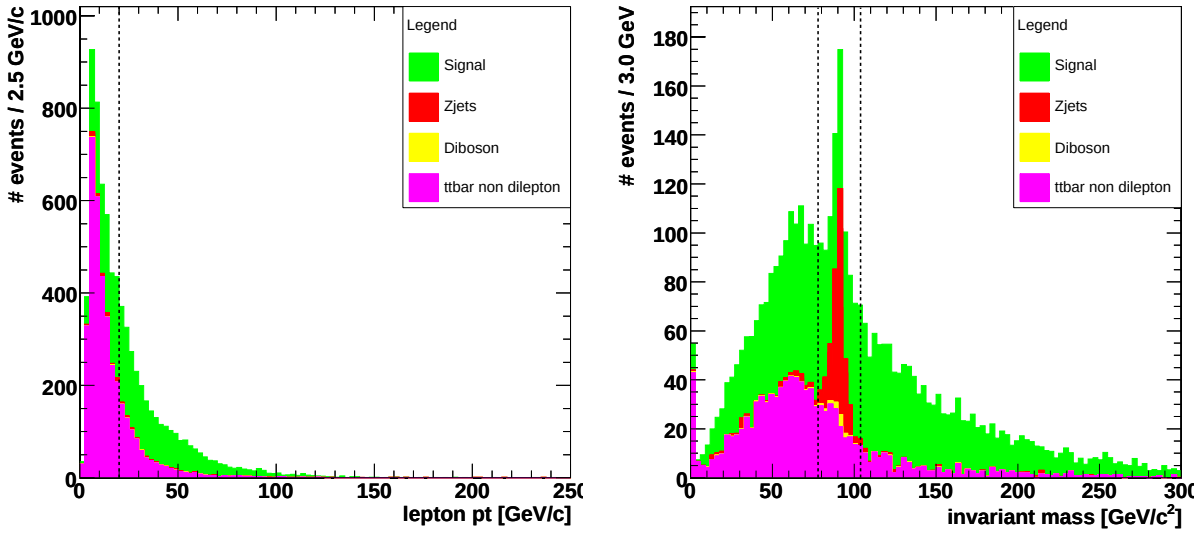

Figure 2: Scaled to $1\ \mathrm{fb}^{-1}$ with all cuts applied, except (left plot) the second (lower) lepton pt cut, or (right plot) the Z mass veto on the invariant mass of both leptons.

The Z mass peak of the invariant mass distribution of two same type leptons is used to remove the contamination due to Z+jet events, as is the requirement for positive btag discriminator values of the two selected jets. The non-dilepton $t\bar{t}$ events usually contain more jets with a p_{T} greater than $30\ \mathrm{GeV}/c$ but do not contain two high p_{T} leptons. The second lepton candidate is considerably softer than the corresponding lepton from the signal decay channel. So a cut on the lower transverse momentum lepton is imposed with $p_{\mathrm{T}} > 20\ \mathrm{GeV}/c$. These cuts are illustrated in the right hand plot of figure 1 and in the plots of figure 2.

The two neutrinos in the decay of the Ws lead to significant missing transverse energy (MET) whereas the decay of Zs into electrons or muons does not generate MET. So a cut on MET to be greater than $40\ \mathrm{GeV}$ improves the signal to background ratio.

Table 1: Selection cuts for the signal and considered background samples. All numbers represent the cumulative accepted cross sections in pb and can be scaled with a factor of 1000 to get the expected number of events in 1/fb.

	$t\bar{t}$ dilepton	other $t\bar{t}$	$Z+\text{jets}$	ZZ	ZW	WW	$S:B$
Before selection	54.22	433.78	11055.30	11.10	0.89	7.74	0.005
L1	45.06	302.34	2967.13	3.09	0.49	6.06	0.014
HLT	36.41	184.43	2007.67	1.55	0.39	4.96	0.017
2 jets	25.92	151.23	194.73	0.45	0.04	0.91	0.075
2 leptons	14.96	24.95	123.26	0.20	0.02	0.24	0.101
isolated leptons	9.60	4.22	48.33	0.10	0.01	0.13	0.182
2 bjets	5.30	3.13	2.55	0.02	0.0005	0.01	0.928
lepton inv. mass	4.46	2.88	0.55	0.004	0.0001	0.01	1.292
lepton pt cut	3.07	0.62	0.34	0.003	0.0001	0.01	3.151
$\not{E}_{\mathrm{T}}$ cut	2.30	0.43	0.05	0.001	0.0001	0.01	4.748
# high p_{T} jet cut	1.85	0.21	0.03	0.001	0.00004	0.007	7.332
kinematical reco.	0.66	0.05	0.002	< 0.001	< 0.00004	< 0.007	12.167

After cuts about 1800 signal events are left with a signal over background ratio of $7.33:1$ as shown in table 1.

The kinematics of the $t\bar{t}$ dilepton events yield an underconstrained equation system due to the two undetected neutrinos in the final state. However if all other kinematic quantities have been measured it is possible to make a fit imposing m_W and assuming a top mass parameter in the range of 100 to $300\ \mathrm{GeV}/c^2$. A weight can then be assigned to the different solutions obtained (see section 2.1.2). The event topology of most of the background events passing the previous cuts does not satisfy the dilepton kinematical constraints. Therefore the actual computation of a mass estimate in the range of 100 to $300\ \mathrm{GeV}/c^2$ further reduces the background and raises the signal over background ratio to about $S:B=12.2:1$ as can be seen in the last line of table 1 and in figure 3.

An event selection for $0.1\ \mathrm{fb}^{-1}$ without relying on any vertex information from the pixel detector, as it might not be installed during the start up phase, and hence no combined b-tagging, is currently under investigation. First results suggest that a signal over background ratio of about $1:1$ is possible before kinematical event reconstruction.

2.1.2 Kinematical event reconstruction

The $t\bar{t}$-system can be reconstructed from the visible final state particles and either the predicted standard model neutrino energy spectrum or the knowledge of the top mass itself. The event kinematics consist of four equations from the invariant masses of the decaying top quarks (eq. 5 and eq. 6) and W-bosons (eq. 3 and eq. 4). Assuming momentum conservation in the transverse plane neglecting ISR or initial transverse momentum of the partons two more equations can be added to the equation system (eq. 1 and eq. 2).

$$0 = p_x^{l^+} + p_x^{l^-} + p_x^b + p_x^{\bar{b}} + p_x^\nu + p_x^{\bar{\nu}} \quad (1)$$

$$0 = p_y^{l^+} + p_y^{l^-} + p_y^b + p_y^{\bar{b}} + p_y^\nu + p_y^{\bar{\nu}} \quad (2)$$

$$m_{W^+}^2 = (E^{l^+} + E^\nu)^2 - \sum_i (p_i^{l^+} + p_i^\nu)^2 \quad (3)$$

$$m_{W^-}^2 = (E^{l^-} + E^{\bar{\nu}})^2 - \sum_i (p_i^{l^-} + p_i^{\bar{\nu}})^2 \quad (4)$$

$$m_t^2 = (E^{l^+} + E^\nu + E^b)^2 - \sum_i (p_i^{l^+} + p_i^\nu + p_i^b)^2 \quad (5)$$

$$m_{\bar{t}}^2 = (E^{l^-} + E^{\bar{\nu}} + E^{\bar{b}})^2 - \sum_i (p_i^{l^-} + p_i^{\bar{\nu}} + p_i^{\bar{b}})^2 \quad (6)$$

Six components of the neutrino momenta are unknown and likewise the top mass in case of a top mass measurement. Nevertheless the equation system can be simplified to a single fourth order polynomial in one of the unknown neutrino components (eq. 7). Its coefficients depend on the visible particles momenta and the top mass. Assuming a value for the top mass as a parameter of the polynomial it can be solved up to a fourfold ambiguity. All other values can then be computed from one of the solutions.

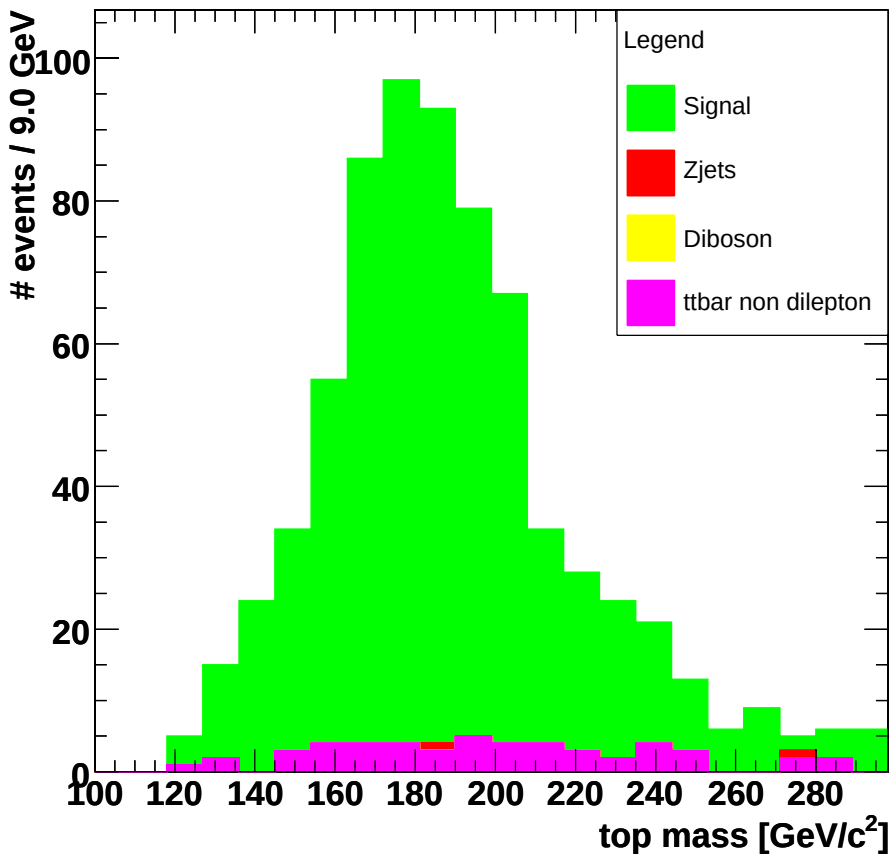

Figure 3: Most Likely top mass after selection for $1\ \mathrm{fb}^{-1}$.

$$0 = \sum_{i=0}^{4} c_i(M_t, p^{l\pm}, p^b, p^{\bar{b}})(p_x^{\bar{\nu}})^i \tag{7}$$

With the knowledge of the top mass and perfect choice, i.e. direct comparison of the up to four different solutions with the MC generator neutrino four momenta, the correlation between generated MC data and the kinematical reconstruction is about 95% (see left hand plot in figure 4). The correlation is not 100% due to neglected ISR and top width effects.

To measure the top mass the event can be kinematically reconstructed by varying the top mass parameter in the polynomial in an interval, e.g. stepping through an interval from $100\ \mathrm{GeV}$ to $300\ \mathrm{GeV}/c^2$ in $1\ \mathrm{GeV}/c^2$ steps and weighting of the different (up to four times two hundred) solutions. The solvability, i.e. the probability normalised to the number of events to find at least one real solution to the polynomial depends on the assumed top mass parameter (see right hand side of figure 4). Below a value equal to the W mass the solvability equals zero, since the equation system assumes a real W boson from the top decay.

2.1.3 Mass determination

The different kinematically possible neutrino solutions from the kinematical equation system are weighted using Standard Model predictions for the energy spectra of the neutrino and antineutrino. These spectra have been computed for every top mass parameter in the range of $100\ \mathrm{GeV}/c^2$ to $300\ \mathrm{GeV}/c^2$ in $1\ \mathrm{GeV}/c^2$ steps corresponding to the parameter choices when stepping through the interval. The neutrino solution with the highest weight is chosen and the appropriate top mass of this solution is then the most probable top mass for the examined event.

The distribution of these most probable top masses for a sample of generated top pair decays yields the most likely top mass (see figure 5 left). Using samples generated with a different top mass the correlation between the reconstructed mass and the generator mass can be plotted (see figure 5 right) resulting in a linear correlation.

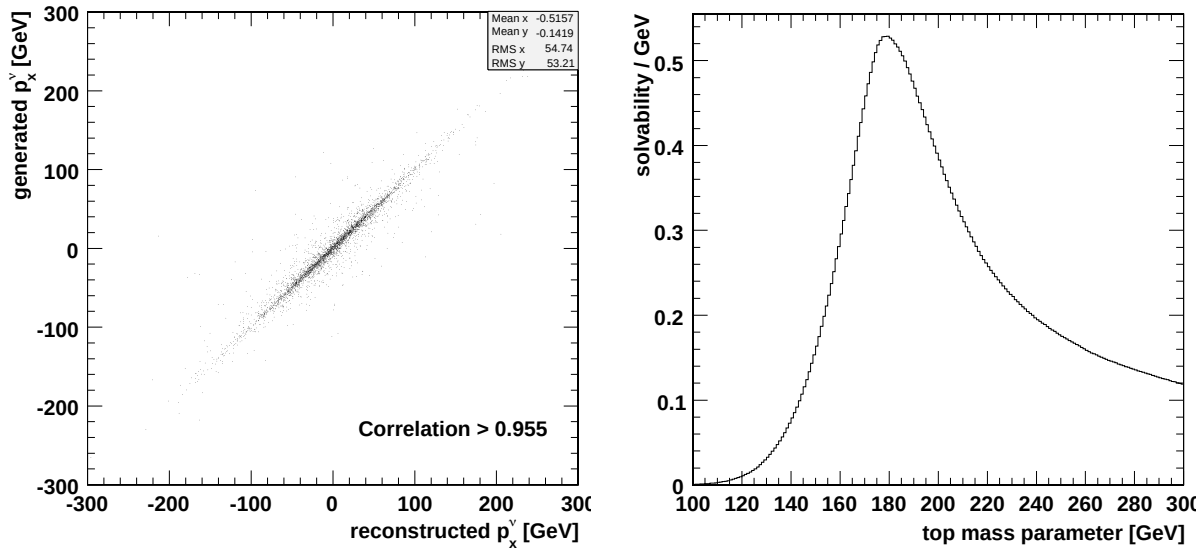

Figure 4: Left: generated neutrino p_x versus reconstructed neutrino p_x. Right: Solvability of the kinematic equation system (both plots use generator level data with $m_t = 175\ \mathrm{GeV}/c^2$).

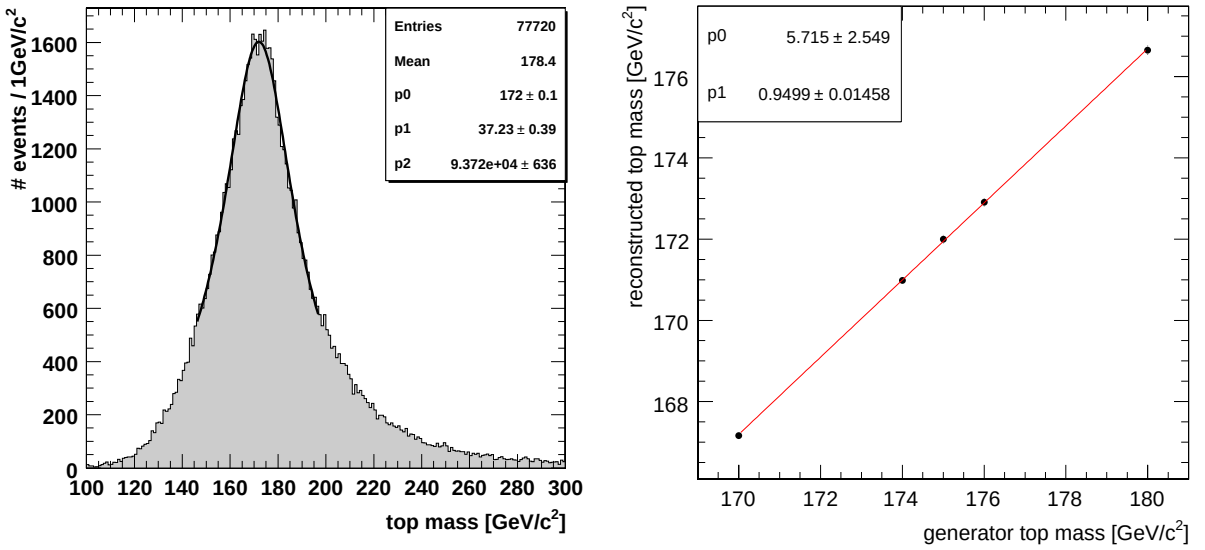

Figure 5: Left: Most likely top mass (generator level; fit parameter $p0$ corresponds to the mean value whereas $p1$ is the full width at half maximum). Right: Correlation between MC top mass and most likely top mass (generator level)

Applying the same method for detector simulated and reconstructed events selected with the cuts from section 2.1.1 gives an estimator for the top mass in the dilepton channel. For $1\ \mathrm{fb}^{-1}$ a Gaussian fit to the signal in a range corresponding to bins with contents above 40% of the maximum yields

$$m_t = (178.5 \pm 1.5)\ \mathrm{GeV}/c^2$$

as illustrated in figure 6 for an input top mass of $175\ \mathrm{GeV}/c^2$. The remaining background is essentially flat as shown in figure 3 and does not affect the mass determination significantly.

2.1.4 Systematics

The main systematic uncertainties on the mass determination in the dilepton channel are due to the approximations used in the kinematic fit and detector effects.

Initial and final state radiation effects modify the kinematics of the process, e.g. the transverse momentum of the $t\bar{t}$

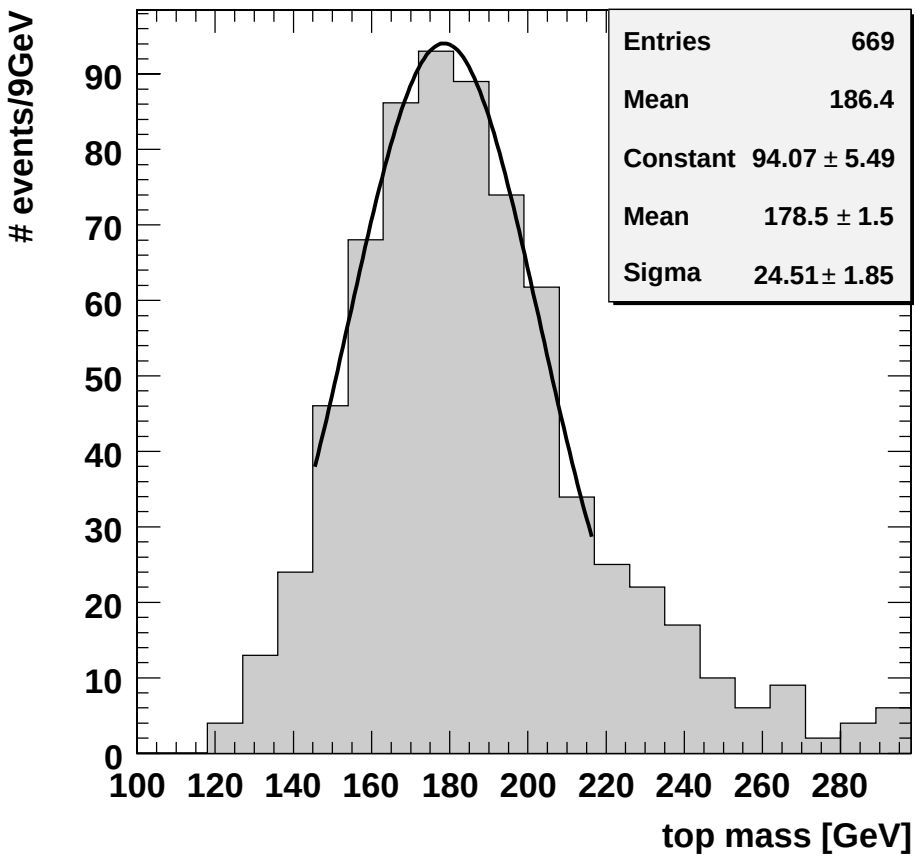

Figure 6: Most Likely top mass after full simulation, reconstruction and selection for $1\ \mathrm{fb}^{-1}$ (signal only).

system. This has a direct influence on the solvability of the equation system and on the neutrino solutions obtained from it. We estimate a systematic shift on the top mass of $\Delta m_t = 0.3\ \mathrm{GeV}/c^2$, following the suggestions of reference [2]. The zero width approximation for both the W bosons and the top quarks in the equation system gives rise to another shift of about $0.1\ \mathrm{GeV}/c^2$.

The most important source of systematic uncertainty arises from uncertainties on the jet energy scale. The expected error after startup (using source calibration and test beam data) is a shift of 15% independent of jet p_T. The corresponding top mass shift amounts to $\Delta m_t = 4.2\ \mathrm{GeV}/c^2$ for integrated luminosities up to $1\ \mathrm{fb}^{-1}$. With better calibration (γ+jet and W fit from the other $t\bar{t}$ channels, see section 2.2.4) this error does reduce to $2.9\ \mathrm{GeV}/c^2$ in a $1 - 10\ \mathrm{fb}^{-1}$ measurement. Further improvements in the knowledge of the jet energy scale (e.g. Z+jet calibration) are expected to lead to a shift of about $1\ \mathrm{GeV}/c^2$ after $10\ \mathrm{fb}^{-1}$ integrated luminosity.

In summary, an early top mass measurement in the dilepton channel will be dominated by jet energy scale uncertainties. Already for an integrated luminosity of $1\ \mathrm{fb}^{-1}$ the statistical error will be half of the systematic one.

2.2 Event Selection for Higher Luminosities

In this section we present a di-lepton selection optimized for high luminosities, of the order of 10 fb^{-1}. Only $e-\mu$ dilepton candidates are considered. The selection of events in this channel requires after trigger selection the presence of just two oppositely charged leptons with $E_{\mathrm{T}} > 20$ GeV in the pseudorapitity ranges $|\eta| < 2.4$ and $|\eta| < 2.5$ for muons and electrons, respectively.

Furthermore, electrons are required to have a ratio between the energies in the hadronic and electromagnetic calorimeter below 0.05, and a ratio between the energy in the electromagnetic calorimeter and the track momentum has to be in the range $(0.8, 3)$. The HLT trigger is based on the presence of **1**μ **or 1**e which cover with high efficiency all the possible final states in this channel. Selection thresholds used in HLT are tightened in the offline lepton selection. Figure 7 shows the muon and electron spectra after applying these selections, comparing the generated and reconstructed distributions. The reconstruction efficiency is good, both for muons and electrons. More than 97% of the generated muons are correctly reconstructed in the considered range, as well as 90% of the electrons with p_{T} above 20 GeV/c.

An electron is considered isolated if the total uncorrected E_{T} of the jets within a cone $\Delta R \leq 0.3$, minus the lepton E_{T}, is $< 30\%$ of the lepton E_{T}. In a similar way a muon is considered isolated, if the sum of the p_{T} of all the tracks present in a cone of $\Delta R \leq 0.3$ minus p_{T} of the μ is less than 2 GeV/c. Figure 8 shows the distribution of these variables for muon and electrons. Here, negative values occur due to the different resolutions of the subdetectors involved in measuring electrons and tracks.

Candidate events must have $\not\!\!E_{\mathrm{T}} > 40$ GeV. The analysis requires at least two jets with uncorrected $E_{\mathrm{T}} > 20$ GeV detected within $|\eta| < 2.5$, where a jet is defined as a fixed-cone cluster with a cone size of $R = 0.5$. Jets produced by electrons are discarded before applying the previous selection by removing those which have an electromagnetic supercluster within $\Delta R = 0.2$ with a ratio between the electromagnetic energy of that supercluster and the uncorrected jet energy above 0.75.

Using these selection cuts, the efficiency at generator level is about 20% and a similar value is obtained at reconstruction level as shown in table 2.

Table 2: Cumulative effect of the different selection criteria applied to the simulated $t\bar{t}$ e-μ di-lepton sample and simulated backgrounds. The column denoted as τ corresponds to a $t\bar{t}$ dilepton sample in which at least one W decays into a τ lepton. Numbers correspond to **LO** accepted cross-sections in pb.

	Signal	τ	WW	WZ	ZZ	Z+jets	other $t\bar{t}$
Before selection	24.3	30.4	7.74	0.89	0.11	3912	438
L1 + HLT	19.4	15.1	4.4	0.37	0.07	657	92
2 jets $E_{\mathrm{T}} > 20$ GeV	11.5	9.8	0.6	0.012	0.006	23.9	73.1
$\not\!\!E_{\mathrm{T}} > 40$ GeV	9.6	8.1	0.5	0.01	0.003	5.8	53.6
Two opposite charged leptons	3.2	0.42	0.04	0.001	0.001	1.17	0.12
b-tagging of two highest E_{T} jets	1.12	0.15	0.002	$\sim 10^{-4}$	$\sim 10^{-5}$	0	0.05

2.2.1 Background estimation

After removal of cosmic-ray muons by timing cuts and photon-conversion electrons as part of the electron selection, the dominant backgrounds to dilepton $t\bar{t}$ events can be divided into two main categories:

a) Physics backgrounds, i.e. , those who have real leptons, real $\not\!\!E_{\mathrm{T}}$ and jets originating from initial or final state radiation, arising mainly from diboson (WW, WZ, and ZZ) + jets production. This category also contains the background coming from top quark decays, either from the semileptonic channel or from tau decays. This kind of backgrounds are expected to be determined using MC simulation.

b) Instrumental backgrounds, characterized in general by their large cross-sections but not having significant $\not\!\!E_{\mathrm{T}}$, among them are: Drell-Yan ($Z/\gamma^{\star} \rightarrow \ell^{+}\ell^{-}$) production, "fake" leptons in $W \rightarrow \ell\nu$ + jet events where a jet is falsely reconstructed as a lepton candidate. In principle it is harder to estimate their contribution to the final sample using MC simulation, then it will be estimated using real data.

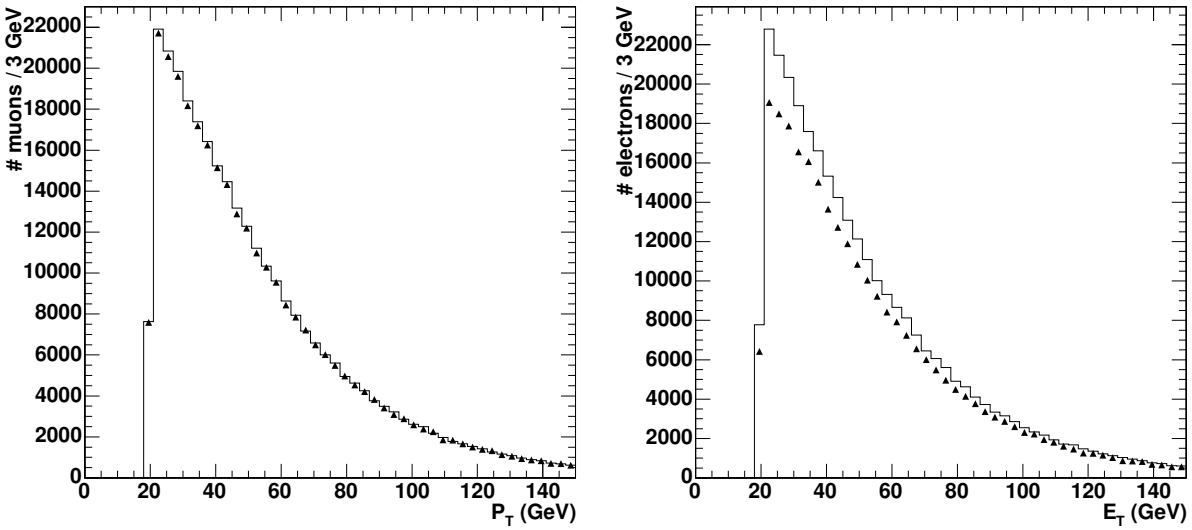

Figure 7: Left: distribution of reconstructed μ p_{T} (dots) compared with respect to their generated μ p_{T} values (solid histogram) for μ selected after a p_{T} cut of $20\ \mathrm{GeV}/c$. Right: distribution of reconstructed electron p_{T} (dots) compared with respect to their generated electron p_{T} (solid histogram) for electron selected after a p_{T} cut of $20\ \mathrm{GeV}/c$.

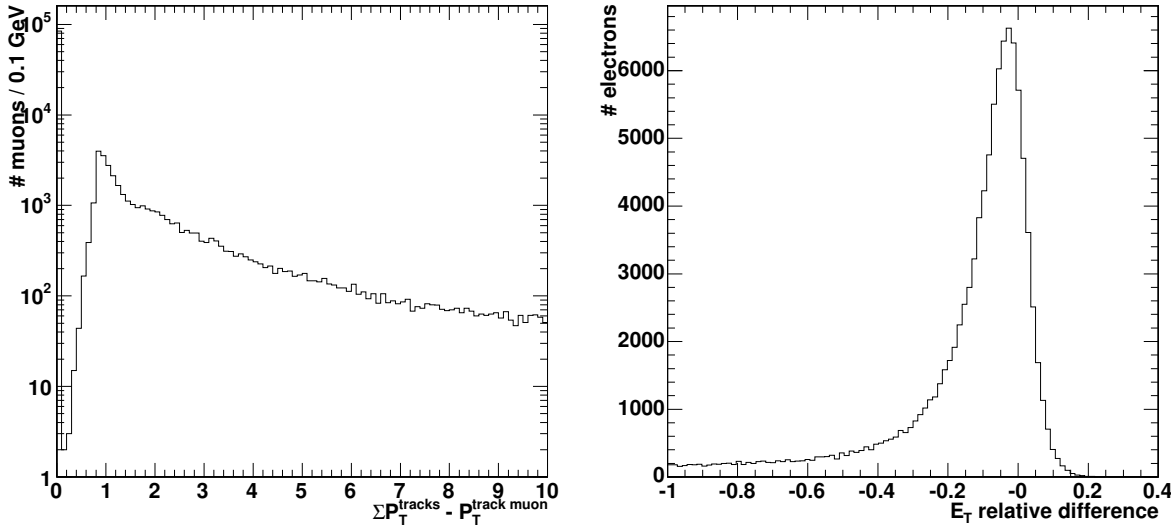

Figure 8: Distribution of variables used in μ (left) and e (right) isolation as described in the text.

2.2.2 b-tagging

In a $t\bar{t}$ event two genuine jets arise from the hadronisation of b quarks. Thus b-tagging techniques are used to further suppress backgrounds in which no jets from b-quarks are present. The technique used is based on the explicit reconstruction of a secondary vertex (SV) in a jet [1]. A variable combining several variables, like the mass of the charged particles associated to the vertex and the distance between the positions of primary and secondary vertices, is computed for all the jets in an event. The distribution of this variable for the three possible types of jet categories, no reconstructed SV, pseudo SV (tracks with significant impact parameter but no reconstructed SV), and reconstructed SV, as defined in [1], is used to tag jets as coming from a b-quark. Candidate events must have at least a value of 1 in each of the two jets selected.

2.2.3 Selection efficiency and cross-section determination

After this selection an efficiency of 5% is obtained, with a very high rejection of all the backgrounds considered at the level of $10^{-3} : 1$ or better, as shown in table 2. A S/B value of 5 is obtained, the main background being the one arising from the dilepton channel in which at least one of the W decays into $\tau\nu_\tau$ and the τ decays leptonically. Events selected in this way are used to determine the total $t\bar{t}$ cross-section.

2.2.4 Systematic uncertainties

Different sources of systematic uncertainties are identified that affect event selection and background determination and thus the cross-section measurement: ISR, FSR, parton distribution functions, b-quark fragmentation, jet energy calibration, lepton identification and isolation, b-tagging efficiency, etc. Detailed studies of these sources have been done based mainly on the results of the studies performed in [3] and [2]. The uncertainty in the amount of initial and final state radiation has been estimated using samples generated with Pythia and simulated and reconstructed with the CMS fast simulation and reconstruction program. Different samples of 2×10^5 events were simulated and reconstructed. In those samples Λ_{QCD} and Q^2_{max} were varied in their recommended range. Their values were controlled by the Pythia parameters $PARP(61)$, $PARP(72)$ and $PARJ(81)$, which were varied in the ranges 0.15 to 0.35 and $PARP(67)$ and $PARP(71)$ which were modified in the ranges 0.25 to 0.4 and 1 to 16 respectively. The uncertainty in the cross-section was taken as coming from the difference in the number of observed events in the samples with the largest difference in the parameters, leading to a 2.5% relative uncertainty in the final value of the cross-section. The uncertainty in the jet energy scale is believed to be one of the most important contributions to the determination of the $t\bar{t}$ cross-section determination. We have modified the heavy quark jet energy scale by a value of $\alpha = 3\%$ modifying the reconstructed momenta using the formula $p^{\mu,jet}_{scaled,\pm\alpha} = (1 \pm \alpha)\, p^{\mu,jet}_{unscaled,\pm\alpha}$ for values of the reconstructed p_{T} higher than 50 GeV/c, and varying linearly from 10% to 3% for p_{T} values ranging from 20 to 50 GeV/c. The relative uncertainty in the cross-section due to this effect has been estimated to be a 3.6% relative value. The effect due to the systematics on $\not\!\!E_{\mathrm{T}}$ has been estimated using a 5% uncertainty in this quantity, that leads to a relative 1.1% uncertainty in the cross-section estimation. The effect due to the uncertainty in b-tag efficiency has been estimated by varying the values of the jet b-tag combined variable by a value of 4% and 5% in the barrel ($|\eta| < 1.5$) and endcaps ($|\eta| > 1.5$) according to the estimations given in [3] for an integrated luminosity of 10 fb^{-1} leading to a 3.8% relative uncertainty in the cross-section estimation. Values of 1% and 0.5% have been conservatively taken as uncertainties coming from electron and muon reconstruction and identification, leading to a 1.6% relative uncertainty in the cross-section estimation. Most of the estimations above are statistically dominated. Checks have been done on events selected with looser selection criteria to increase the confidence on these estimations. Other systematic effects have been studied, as in the case of ISR and FSR mainly using samples generated with the CMS fast simulation program, according to the suggestions given in [2]. Among them, we have considered the following effects. Taking a 30% difference between samples with and without in-time pile-up for the low luminosity regime ($\mathcal{L} = 2 \times 10^{33}$ cm^{-2} s^{-1}) leads to a 3.6% relative uncertainty in the cross-section value. The Underlying Event description has been studied by simulating samples with different values of the color screening cut-off parameter, that correspond to the $PARP(82)$ value in the Pythia generator. This value has been varied in the range 2.4 to 3.4 leading to a 4.1% relative uncertainty in the cross-section. The uncertainty coming from hadronization and fragmentation was estimated by varying the Lund b parameter and σ_q. Samples were simulated with values of $PARJ(42)$ and $PARJ(21)$ within 2σ values of the OPAL central data, leading to a relative uncertainty in the cross-section of 5.1%. Uncertainties arising from PDFs were studied with CTEQ 6M using a reweighting routine that leads to a 5.2% uncertainty in the cross-section determination. The statistical uncertainty in the cross-section determination is about 0.9% for 10 fb^{-1} integrated luminosity. Finally the uncertainty in the cross-section coming from the luminosity estimation was taken as 3% as expected for 10 fb^{-1} integrated luminosity. These numbers lead to

$$\Delta\sigma_{t\bar{t}\ dil\ e/\mu}/\sigma_{t\bar{t}\ dil\ e/\mu} = 11\%\ (\mathrm{syst.}) \pm 0.9\%\ (\mathrm{stat.}) \pm 3\%\ (\mathrm{luminosity})$$

and are summarized in table 3.

2.3 Top decays in tau leptons

Studies are being performed to select events in the final state with τ leptons. In about 21% of the $t\bar{t}$ events, at least one W boson decays into a τ final state. Depending on its decay, the τ lepton can be identified as a narrow jet, an isolated track, or an electron or muon. Two high-energy b jets, missing transverse energy, and the decay products from the second W boson complete the event topology. We consider here di-leptonic $t\bar{t}$ decays with one tau lepton decaying into hadrons in the final state $t\bar{t} \to \mathrm{b\bar{b}}\tau\nu_\tau\ell\nu_\ell,\ (\ell = \mathrm{e}, \mu)$. The primary aim of the analysis is to make a

Table 3: Uncertainties in the $t\bar{t}$ dilepton cross-section determination

Effect	$\Delta\sigma_{t\bar{t}\ dil\ e/\mu}/\sigma_{t\bar{t}\ dil\ e/\mu}$
ISR and FSR	2.5%
Jet Energy Scale	3.6%
b-tag efficiency	3.8%
lepton reconstruction	1.6%
$\not{E}_{\mathrm{T}}$	1.1%
Pile-Up	3.6%
Underlying Event	4.1%
heavy quark fragmentation	5.1%
PDF uncertainties	5.2%
Statistical uncertainty	0.9%
Integrated luminosity	3%

first observation of the final state, containing at least a τ lepton. This will allow to test lepton universality in the whole top decay process. Measuring the ratio $BR(t\bar{t} \rightarrow \ell\tau)/BR(t\bar{t} \rightarrow \ell\ell)$ will allow to set new limits on the presence of non-standard physics in this process. This channel has a special relevance for being not only a source of background for Supersymmetry and Higgs searches, but also for the other dileptonic top channels.

Table 4: Cumulative effect of the different selection criteria applied to simulated $t\bar{t}$ sample. Numbers correspond to accepted **LO** cross-sections.

Cut	Efficiency $\times$ cross sections (pb)			
	tt (signal)	tt(other dilepton)	tt (semileptonic)	tt (hadronic)
All	15.62	38.94	218.88	218.88
Trigger	8.61	25.40	85.90	2.08
2 jets	6.97	18.90	80.08	2.04
$\geq$ 1 Iso lepton	4.27	13.11	34.93	0.11
$\not{E}_{\mathrm{T}} \geq 40$ GeV	3.58	10.89	26.41	0.05
1 lepton	3.48	6.73	25.24	0.04
τ candidate with opposite Q	0.75	0.20	0.75	0.001
b-tagging	0.29	0.07	0.30	0.0005

τ candidates are selected and identified following the method of the MSSM Higgs and HLT analyses [4], adapting the different selection criteria to the momentum range in which τ candidates are expected to be produced in top decays. All tracks with $p_{\mathrm{T}} > 5\ \mathrm{GeV}/c$ are taken as seed tracks except those corresponding to reconstructed electrons. These tracks are marked as seeds if a jet is within the matching cone of $\Delta R = 0.1$ Then, centered on the seed track all tracks with $p_{\mathrm{T}} > 1\ \mathrm{GeV}/c$ are counted in the signal cone which has $\Delta R < 0.09$. Finally, centered on the jet axis tracks in an isolation cone of $\Delta R < 0.3$ are counted. Objects reconstructed in this way are considered as τ candidates if the number of tracks in both countings are the same, i.e. , there is no other track between the signal cone and the isolation cone. Candidates where all tracks have the same electric charge or which have only two tracks are removed as in these cases it is not possible to determine the charge of the reconstructed τ correctly. The hadronic tau identification efficiency extracted from the di-lepton samples is about 30% using this method as can be seen in figure 9. The variation with p_{T}, and η of the fraction of correct assignments of reconstructed τ candidates with respect to generated τ within the di-lepton sample is shown in figure 10

τ candidates reconstructed as described above are used to select $t\bar{t}$ events decaying into dileptons in which one of the leptons is a τ decaying hadronically and the other lepton in the final state is an electron or a μ. The selection proceeds in a similar way as in the dilepton case. The events are selected by requiring the presence of at least two uncalibrated jets with $p_{\mathrm{T}} > 20\ \ \mathrm{GeV}/c$ and $|\eta| < 2.5.$, at least one isolated lepton (electron or μ), selected as described in 2.2, sufficient missing transverse energy, and only one isolated lepton. One isolated tau candidate separated from the isolated lepton has to be present, and the isolated lepton and the tau candidate must have opposite charges. The effect of these selection criteria are described in detail for the $t\bar{t}$ sample in table 4, and for the main backgrounds in 5. The last step in the selection of signal events is the use of the jet combined b-tag variable. Candidate events must have at least a value of 1 in each of the two jets selected. An overall efficiency close to 2% is obtained, with a high rejection power against all backgrounds considered as shown in table 4. A S/B

Table 5: Cumulative effect of the different selection criteria applied to simulated backgrounds. Numbers correspond to accepted **LO** cross-sections.

Cut	Efficiency × cross sections (pb)				
	WW (inclusive)	Z+jets (leptonic)	ZW	QCD(80-120)	QCD(120-170)
All	69.69	1533	26.69	$2.66{\cdot}10^6$	$470.2{\cdot}10^3$
Trigger	39.52	559.24	10.99	7980.00	1410.60
2 jets	24.65	125.18	4.77	5506.20	1116.74
≥ 1 Iso lepton	4.89	62.89	0.57	38.90	17.72
$\not{E}_{\rm T} \geq 40$ GeV	3.54	17.60	0.32	11.57	6.12
1 lepton	3.31	11.08	0.28	10.97	5.61
τ candidate with opposite Q	0.14	0.91	0.011	0.20	0.11
b-tagging	0.006	0.03	0.0002	0.00	0.00

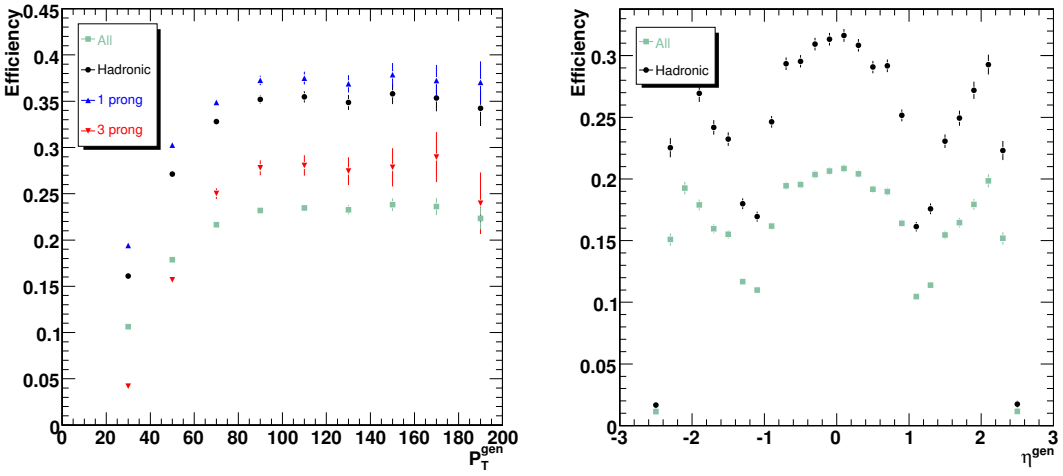

Figure 9: Reconstruction efficiency of τ candidates as a function of $p_{\rm T}$, and η.

value close to 1 is obtained, the main background being the one arising from the $t\bar{t}$ semileptonic channel.

2.3.1 Systematic uncertainties

The majority of the systematic uncertainties are described in 2.2.4. There is another systematic uncertainty intrinsic to this analysis due to the τ reconstruction and identification. The τ detection is affected by the requirements imposed on the tracks and π^0 in the isolation cone. Also the uncertainty in the energy scale uncertainty affects the τ cluster energy definition. The multiple interaction and pile up events affect the number of tracks in the signal and isolation cone. Based on preliminary studies, we assigned a 12% uncertainty to the τ reconstruction and identification. The statistical uncertainty in the cross-section determination is about 1.3% for an integrated luminosity of $10\ \ {\rm fb}^{-1}$. Then combining these values with those estimated in the previous section, the relative uncertainty in the estimation of the cross-section can be written as:

$$\Delta\sigma_{t\bar{t}\ dil\ \tau,e\mu}/\sigma_{t\bar{t}\ dil\ \tau,e\mu} = 16\%\ (\text{syst.}) \pm 1.3\%\ (\text{stat.}) \pm 3\%\ (\text{luminosity})$$

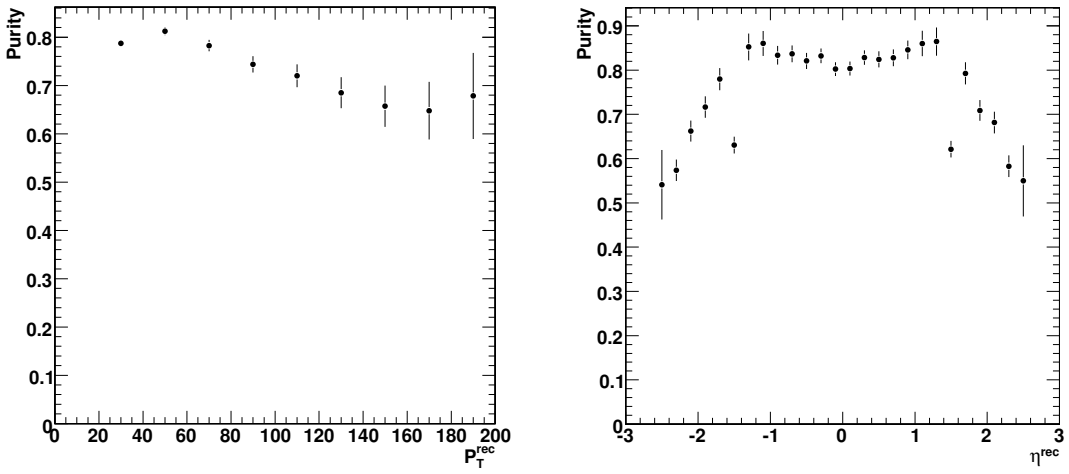

Figure 10: Fraction of correct assignments in the reconstruction of τ candidates within the di-lepton channel as a function of p_{T}, and η.

3 Selection of Fully Hadronic Events

The fully hadronic final state, characterized by the nominal six-jets topology $t\bar{t} \rightarrow WW\mathrm{b\bar{b}} \rightarrow qqqq\mathrm{b\bar{b}}$, has the largest branching fraction (46%), and kinematics that can be fully reconstructed. However, this channel is affected by a large background from QCD multi-jet production, which makes the isolation of the signal rather challenging. Improvements in the signal-to-background ratio are possible by requiring the presence of b-quark jets and by selecting central and very high-energy kinematic configurations which are expected for jets arising from the decay of a massive object like the top quark. A specific multi-jet trigger that uses b-tagging information has been devised for this analysis and an optimized selection has been applied.

For the analysis, event samples generated with PYTHIA have been used. The signal consists of 500000 inclusive $t\bar{t}$ events, from which a subsample of 230000 fully hadronic $t\bar{t}$ events is extracted. The background consists of 1500000 multi-jet events (QCD) generated with $50 < \hat{p_{\mathrm{T}}} < 470\ \mathrm{GeV}/c$, where the $\hat{p_{\mathrm{T}}}$ symbol indicates the transverse momentum of the most energetic parton of the hard scattering before the final-state radiation processes.

3.1 Trigger Preselection

The trigger selection uses the inclusive jet trigger envisaged in [5], which considers multi-jets with different E_{T} thresholds depending on the number of jets, up to 4 jets, and a special inclusive b-jet trigger [6], implemented according to the following criteria:

- Level-2: jet reconstruction with the following minimal E_{T} thresholds:
  1-jet or 2-jet events: 350 GeV E_{T} for highest-E_{T} jet
  3-jet events: all 3 jest with at least 150 GeV E_{T}
  4-jet events: all 4 jets with at least 55 GeV E_{T}

- Level-2.5: b-tagging based on fast pixel track and vertex reconstruction as ingredients, on the two most energetic jets requiring 2 tracks with impact parameter significance exceeding 2σ;

- Level-3: b-tagging based on regional full track reconstruction and same vertex reconstruction as ingredients, on the two most energetic jets requiring 3 tracks with impact parameter significance exceeding 2.5σ.

The jets are reconstructed with an iterative cone algorithm with a fixed cone size of 0.5 and are calibrated using γ+jet events. The b-tagging algorithm is based on the impact parameters of charged particle tracks and exploits the lifetime properties of weakly-decaying b-hadrons.

The trigger requires either multiple jets in the event (n-jet) or a b-tagged jet among the two highest-E_{T} jets (b-jet).

The rates and the effective cross sections, respectively for the QCD and $t\bar{t}$ fully hadronic events, at the production and at the different levels of the trigger selection, are given in Table 6. The signal efficiencies are also reported. The b-jet stream significantly improves the efficiency of the inclusive jets stream for fully hadronic final states (15%).

After the trigger selection the QCD rate is reduced to 23 Hz, the signal efficiency is 16.8% and the signal to background ratio, S/B, amounts to 1/300.

3.2 Event Selection

The $t\bar{t}$ fully hadronic efficiency (factorizing out the trigger efficiency) and the QCD rate are shown in Figure 11 as a function of the jet transverse energy cut for different values of the minimum number of jets considered. A discriminant selection is needed in order to improve the signal to background ratio. Different choices on the minimum number of jets and jet transverse energy are possible as shown in the figures.

The optimal selection is based on the best statistical significance of the signal achievable, defined as $S/\sqrt{S+B}$, for an integrated luminosity of $\mathcal{L} = 1\ \mathrm{fb}^{-1}$.

The first step of the selection requires a topology of $6 \leq N_{jet} \leq 8$, consistent with the basic physical process considered and taking into account possible additional jets from final state radiation. For a jet to be counted, the jet pseudorapidity must satisfy $|\eta| < 2.4$ and its transverse energy must be greater than 30 GeV. The effective cross section of $t\bar{t}$ and QCD events for minimum jet transverse energy of $E_{\mathrm{T}} > 30$ GeV is represented in Figure 12 as a function of the number of jets.

Table 6: QCD rates and effective cross-sections (a) and $t\bar{t}$ fully hadronic rates, effective cross-sections and efficiencies (b), at production level and at different levels of trigger selection (Level-1, HLT b-jet stream, n-jet stream and n-jet-or-b-jet). Details on single QCD $\hat{p_T}$ rates are also given in (c).

Channel	QCD $50 < \hat{p_{\mathrm{T}}} < 470$ GeV/c				
	Production	Level-1	HLT		
			b-jet	n-jet	n-jet + b-jet
Rate [Hz]	49k	3.3k	19.4	6.3	**23.2**
$\sigma\epsilon$ [pb]	25M	1.7M	9.7k	3.2k	**11600**

(a)

Channel	$t\bar{t} \rightarrow qqqq\mathrm{b\bar{b}}$				
	Production	Level-1	HLT		
			b-jet	n-jet	n-jet + b-jet
Rate [Hz]	0.45	0.26	0.07	0.02	**0.08**
$\sigma\epsilon$ [pb]	225	130	34	10	**38**
Efficiency (%)	100	57.2	14.9	4.4	**16.8**

(b)

Channel	Rate [Hz]				
QCD $\hat{p_T}$	Production	Level-1	HLT		
			b-jet	n-jet	n-jet + b-jet
50 ÷ 80	42 k	2 k	0	0	0
80 ÷ 120	5.9 k	752	1.6	0.2	1.8
120 ÷ 170	1 k	372	4.0	0.7	4.5
170 ÷ 230	202	141	4.3	1.6	5.4
230 ÷ 300	47.7	44.3	3.5	1.8	4.6
300 ÷ 380	12.8	12.7	3.8	1.3	4.4
380 ÷ 470	3.8	3.8	2.2	0.7	2.5

(c)

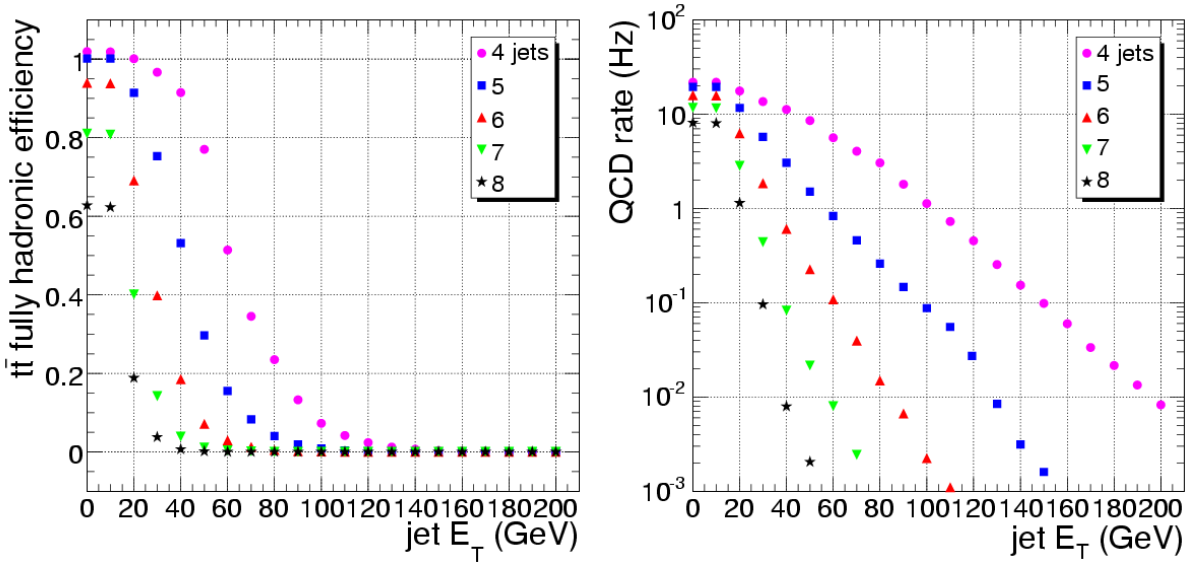

Figure 11: $t\bar{t}$ fully hadronic efficiency (left) and QCD rate (right) as a function of jet transverse energy for different values of the minimum number of jets considered, after the trigger selection.

Different variables of shape in the phase space, potentially able to separate the signal from the background are then taken into account. The useful variables with the corresponding cuts applied in sequence are:

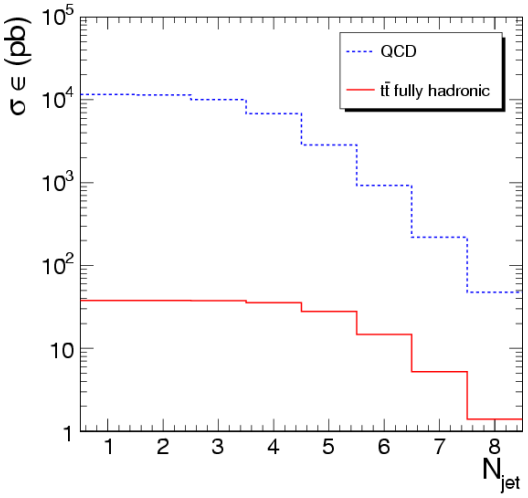

Figure 12: Effective cross section of $t\bar{t}$ and QCD events as a function of the number of jets for a request of minimum jet transverse energy $E_{\mathrm{T}} > 30$ GeV.

- centrality, $\mathcal{C} \geq 0.68$, where $\mathcal{C}$ is the fraction of the hard scatter energy going in the transverse plane $\sum E_{\mathrm{T}}/\sqrt{\hat{s}}$. Here, $\hat{s} = (\sum E)^2 - (\sum Pz)^2$, and all sums here and in the following run over the reconstructed jets
- aplanarity, $\mathcal{A} \geq 0.024$, where $\mathcal{A} = \frac{3}{2}Q_1$, Q_1 being the smallest of the three normalized eigenvalues of the sphericity tensor $M_{ab} = \sum_j P_{ja}P_{jb}$
- non-leading jet total transverse energy obtained removing the two most energetic jets $\sum E_{\mathrm{T}} - E_{\mathrm{T}}(1) - E_{\mathrm{T}}(2) = \sum_3 E_{\mathrm{T}} \geq 148$ GeV

The distributions of these variables for $t\bar{t}$ and QCD events are shown in Figure 13.

After the selection a b-tagging is applied to the surviving samples of $t\bar{t}$ all-hadronic and QCD events. Selection criteria of at least one b-jet and of two b-jets are considered.

Table 7 lists the $t\bar{t}$ fully hadronic and QCD effective cross sections, the signal to background ratio, the statistical significance (referred to $\mathcal{L} = 1$ fb^{-1}) and the $t\bar{t}$ fully hadronic efficiency at each step of the selection (applied in cascade) starting from values obtained after the trigger selection. After the selection and b-jet requirement, the signal to background ratio amounts to 1/17 (1/9) respectively for 1 (2) b-tag samples, for a signal efficiency of 3.8% (2.7%) relative to the fully-hadronic $t\bar{t}$ sample.

Table 7: Selection steps with the corresponding $t\bar{t}$ and QCD effective cross sections, signal to background ratio, statistical significance achieved and $t\bar{t}$ fully hadronic efficiency.

Selection	Requirement	$\sigma\epsilon_{t\bar{t}}$ [pb]	$\sigma\epsilon_{QCD}$ [pb]	S/B	$S/\sqrt{S+B}$ ($\mathcal{L} = 1$ fb^{-1})	$\epsilon_{t\bar{t}}$ (%)
Trigger	HLT jet+b-tagging	38	11600	1/300	11.1	16.8
Event	$6 \leq N_{jet} \leq 8$	35	7900	1/225	12.4	15.5
	$E_{\mathrm{T}} \geq 30$ GeV	15	930	1/60	15.4	6.6
	centrality ≥ 0.68	9.9	324	1/33	17.1	4.4
	aplanarity ≥ 0.024	9.0	251	1/28	17.7	4.0
	$\sum_3 E_{\mathrm{T}} \geq 148$ GeV	9.0	229	1/25	18.4	4.0
b-tagging	1 b-tag	8.6	148	**1/17**	21.7	**3.8**
	2 b-tag	6.0	54	**1/9**	24.1	**2.7**

3.3 Cross Section Expectation and Systematic Uncertainties

The signal efficiency relative to the total inclusive $t\bar{t}$ sample, to be used in the calculation of the total $t\bar{t}$ production cross section, becomes 2.3% (1.6%), respectively for the 1 (2) b-tag requirement.

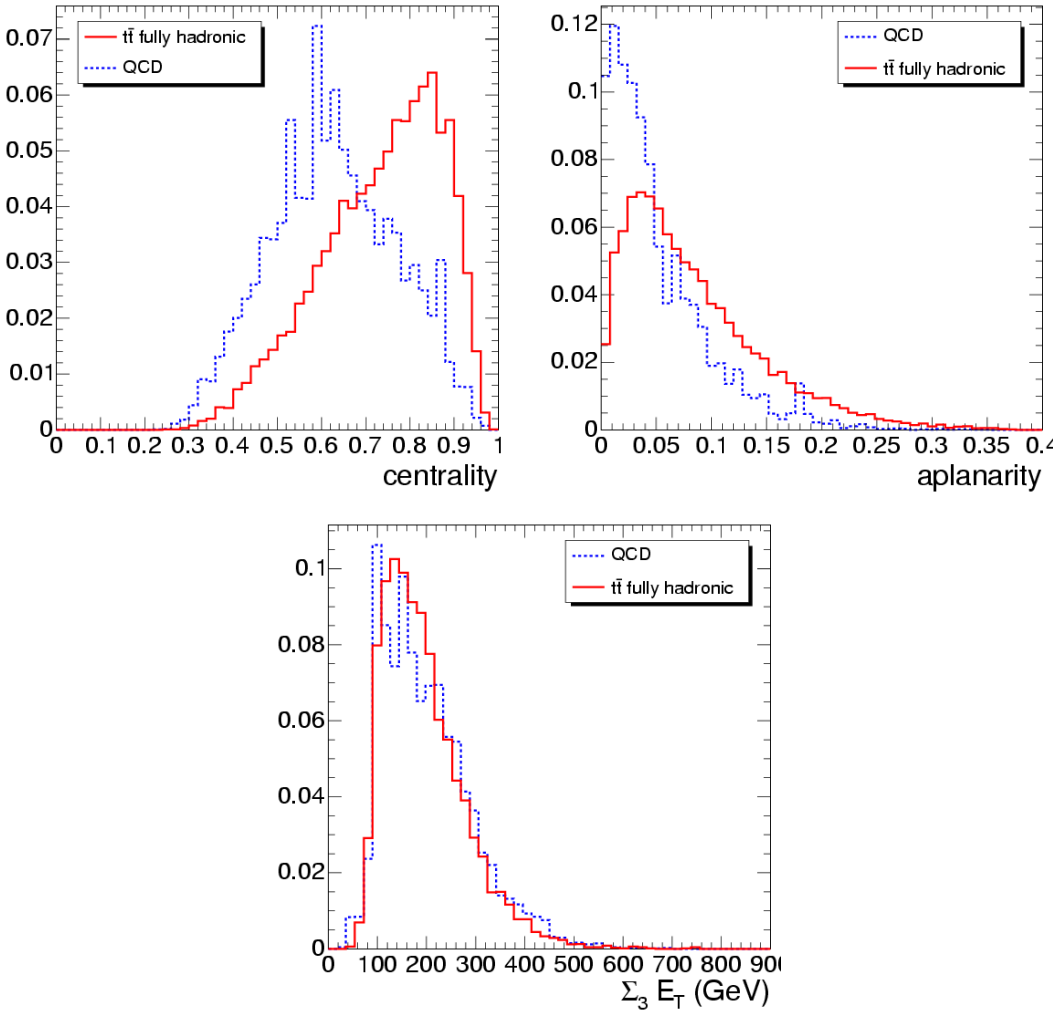

Figure 13: Distributions of centrality (left), aplanarity (right) and $\sum_3 E_{\mathrm{T}}$ (bottom) for $t\bar{t}$ and QCD events (normalized to the same area).

The estimated statistical uncertainty on the cross section is reported in Table 8, with the expected number of signal and background events, for an integrated luminosity $\mathcal{L} = 1\ \mathrm{fb}^{-1}$.

In addition to the statistical uncertainties, significant systematic uncertainties on the signal efficiency (fragmentation model, PDF, ISR/FSR, jet energy scale, b-tagging), the expected background, and the integrated luminosity, are expected. The fine-tuning of the optimized selection will be derived considering these uncertainties.

Sources of systematic uncertainty are studied as described in detail in Section 2.2.4. From the experience of CDF and DØ experiments at Tevatron [7], one of the dominating systematic uncertainties arises from the uncertainty on the jet energy scale. This contribution, evaluated according to the functional form given in [8], amounts to about 11.2%.

The systematic uncertainty related with the trigger selection is calculated considering contributions from b-tagging and jet energy scale. The b-tagging efficiency is measured using two independent triggers, muon and b-jet, applied to inclusive $t\bar{t}$ events, and counting events triggered by single stream and doubles/both stream. This gives a relative uncertainty below to 5%.

Table 9 summarizes the contributions due to the total uncertainty on the cross section, which combined lead to a relative uncertainty of:

$$\Delta\sigma/\sigma = 3\%\ (\mathrm{stat.}) + 20\%\ (\mathrm{syst.}) + 5\%\ (\mathrm{luminosity})$$

Table 8: Number of $t\bar{t}$ and QCD events, $t\bar{t}$ efficiency, absolute and relative statistical uncertainties expected on the cross section measurement for an integrated luminosity of $1\ \mathrm{fb}^{-1}$.

Requirement	$\mathcal{L} = 1\ \mathrm{fb}^{-1}$				
	events $t\bar{t}$	events QCD	ϵ (%)	$(\Delta\sigma)_{\mathrm{stat}}$ [pb]	$(\Delta\sigma/\sigma)_{\mathrm{stat}}$ (%)
1 b-tag	11500	148000	**2.3**	**17**	**3.5**
2 b-tag	8000	54000	**1.6**	**15**	**3.0**

Table 9: Systematic uncertainty contributions to the cross section measurement.

	$\Delta\sigma/\sigma$ (%)
HLT	5.9
Pile Up	10.0
Underlying Event	4.1
Fragmentation	1.9
PDF	4.2
IS/FS Radiation	7.9
Jet Energy Scale	11.2
b-tagging	2.0
Background	5.0
Integrated Luminosity	5.0
Statistical Uncertainty ($1\ \mathrm{fb}^{-1}$)	3.0

3.4 Event selection based on neural net

A more refined selection can be based on a neural net exploiting the same variables considered so far. Such approach is attempted in order to investigate the possibility of improving the S/B ratio and/or the efficiency.

Due to systematics related with the Monte Carlo description of the background, both approaches are considered. The previous selection which will be called "early" selection could represent a more conservative approach for the first LHC analyses.

The neural net used for the analysis is the Multilayer perceptron (MLP) implemented inside ROOT[9] through the class *TMultiLayerPerceptron*. This is a simple feed-forward network with an input layer, some hidden layer and an output layer. In this implementation one single hidden layer with $2n$ nodes, being n the number of input variables, is used. One single output node, which provides a convenient selection variable to cut on, is chosen.

The training is made on subsets of the $t\bar{t}$ and QCD samples containing the same number of events. For this purpose the QCD datasets are weighted using the correspondent effective cross section and merged. The learning method used is the Broyden, Fletcher, Goldfarb, Shanno (BFGS) method. The neural net is then applied on the whole sample of signal ($t\bar{t}$) and background (QCD) events.

Different neural network configurations have been applied and studied starting from events satisfying the topology request of $6 \leq N_{jet} \leq 8$ (jet pseudorapidity $|\eta| < 2.4$). Different cuts on jet transverse energy are considered.

The most effective among the studied neural net configurations is the one referring to the signal and background samples after a cut on jet transverse energy of $E_{\mathrm{T}} > 25\ \mathrm{GeV}$ and consists of 6 input nodes:

- E_{T} 1st jet
- E_{T} 6th jet
- Centrality
- Aplanarity
- $\sum_3 E_{\mathrm{T}}$
- Sphericity

which are the same variables used for the "early" selection, plus the sphericity and transverse energy of the first and 6th jet, where jets are ordered by E_{T}.

The output of the training is shown in Figure 14. In Figure 15 a layout of the network, where the thickness of the lines is proportional to the weight, and the difference between background and signal for each input variable are shown.

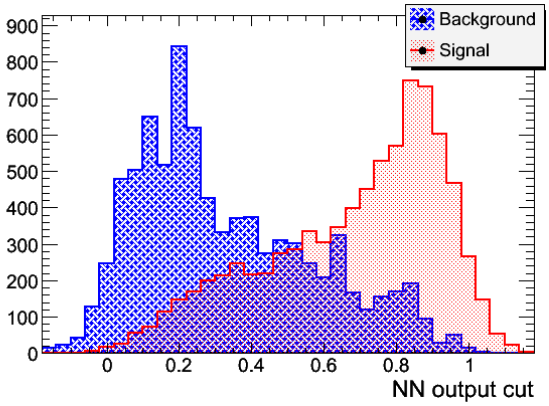

Figure 14: Output of the neural net after the training as evaluated on a "test" sample containing the same number of $t\bar{t}$ and QCD events.

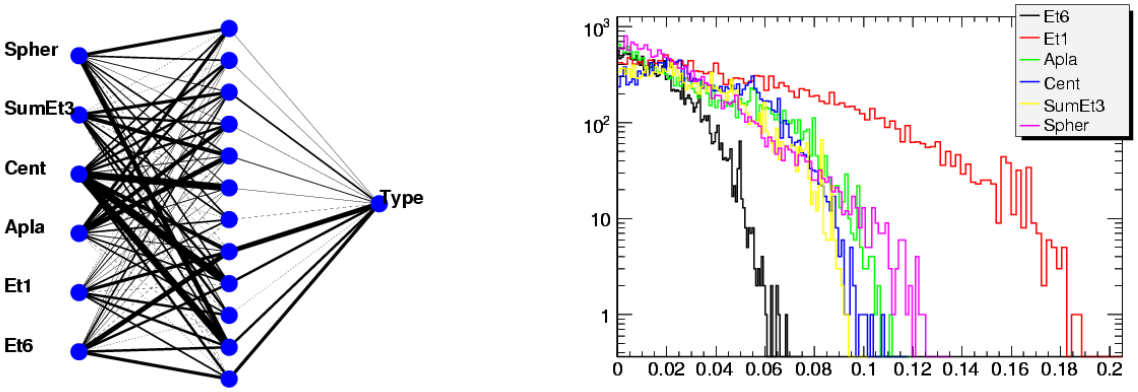

Figure 15: Neural net description (left) where the thickness of the lines is proportional to the weight, and differences between background and signal variables (right) where units on the x-axis are arbitrary.

The output distributions when the neural net is applied to the whole sample of $t\bar{t}$ and QCD events are shown in Figure 16.

The performance of the neural net is quantified in Figure 17. The signal efficiency and the expected S/B ratio as a function of the cut on the neural net output are plotted. Superimposed on the plots are the values corresponding to the "early" selection.

In Figure 18 instead the S/B ratio as a function of the $t\bar{t}$ efficiency is reported. The superimposed point is the value corresponding to the "early" selection. With respect to the "early" selection, the request for a neural net output $\geq$ 0.77 improves the S/B ratio from 1/25 to 1/10 with same effciency (i.e. 4%).

As done after the "early" selection, a b-tagging is applied to the surviving samples of $t\bar{t}$ all-hadronic and QCD events. Selection criteria requiring at least one b-jet or two b-jets are considered.

Table 10 lists the $t\bar{t}$ fully hadronic and QCD effective cross sections, the signal to background ratio, the statistical significance (referred to $\mathcal{L} = 1\ \mathrm{fb}^{-1}$) and the $t\bar{t}$ fully hadronic efficiency at each step of the selection (applied in cascade) starting from values obtained after the trigger selection. The "early" selection cuts are replaced by the neural net. After b-jet requirement, the signal to background ratio amounts to 1/7 (1/3) respectively for 1 (2) b-tag samples, for a signal efficiency of 3.8% (2.7%) relative to the fully-hadronic $t\bar{t}$ sample.

The signal efficiency relative to the total inclusive $t\bar{t}$ sample, to be used in the calculation of the total $t\bar{t}$ production

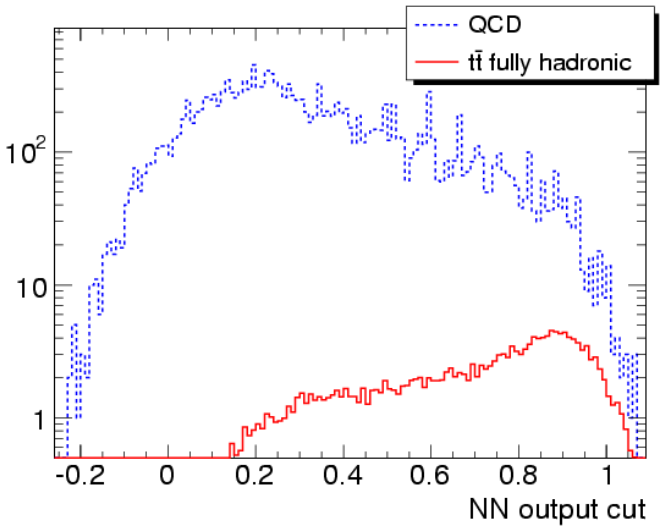

Figure 16: Output of the neural net on the whole sample of $t\bar{t}$ and QCD events. The distributions are normalized to the effective cross section.

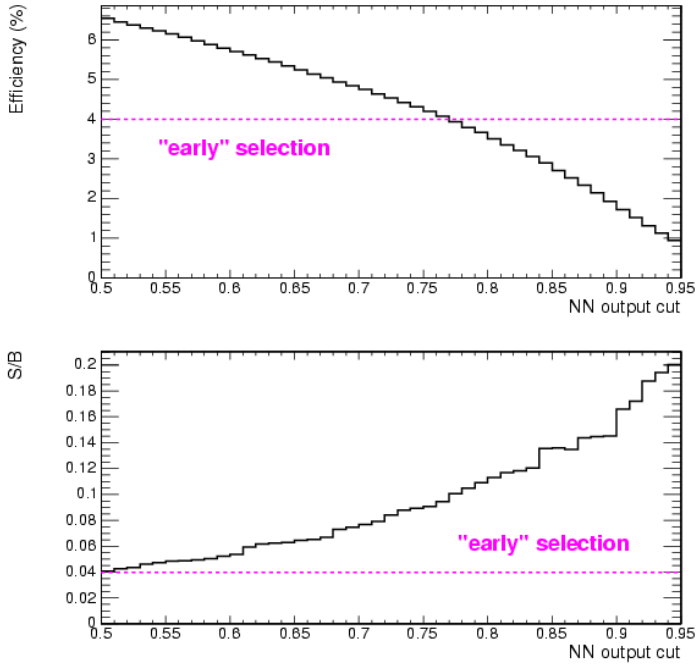

Figure 17: Signal efficiency (top) and S/B ratio (bottom) as a function of the NN output cut. Also shown (dashed lines) are the values for "early" selection.

cross section, becomes 2.3% (1.6%), respectively for the 1 (2) b-tag requirement.

The estimated statistical uncertainty on the cross section is reported in Table 11, with the expected number of signal and background events, for an integrated luminosity $\mathcal{L} = 1\ \mathrm{fb}^{-1}$.

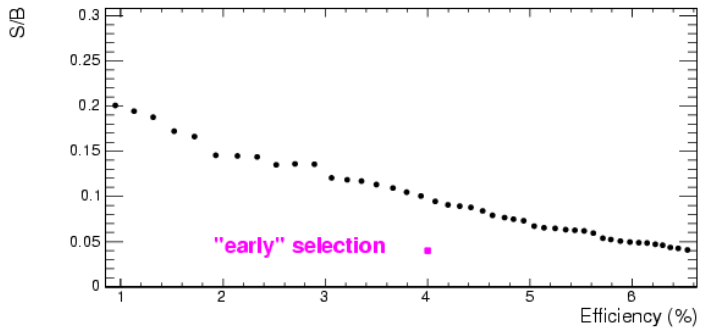

Figure 18: S/B ratio as a function of $t\bar{t}$ efficiency. Also shown (square) is the the values for "early" selection.

Table 10: Selection steps with the corresponding $t\bar{t}$ and QCD effective cross sections, signal to background ratio, statistical significance achieved and $t\bar{t}$ fully hadronic efficiency.

Selection	Requirement	$\sigma\epsilon_{t\bar{t}}$ [pb]	$\sigma\epsilon_{QCD}$ [pb]	S/B	$S/\sqrt{S+B}$ ($\mathcal{L} = 1$ fb^{-1})	$\epsilon_{t\bar{t}}$ (%)
Trigger	HLT jet+b-tagging	38	11600	1/300	11.1	16.8
Event	$6 \leq N_{jet} \leq 8$	35	7900	1/225	12.4	15.5
	$E_{\mathrm{T}} \geq 25$ GeV	20	1650	1/80	15.5	8.7
	neural net	9.0	91	1/10	28.5	4.0
b-tagging	1 b-tag	8.6	61	**1/7**	32.6	**3.8**
	2 b-tag	6.0	20	**1/3**	37.2	**2.7**

Table 11: Number of $t\bar{t}$ and QCD events, $t\bar{t}$ efficiency, absolute and relative statistical uncertainties expected on the cross section measurement for an integrated luminosity of 1 fb^{-1}.

Requirement	$\mathcal{L} = 1$ fb^{-1}				
	events $t\bar{t}$	events QCD	ϵ (%)	$(\Delta\sigma)_{\mathrm{stat}}$ [pb]	$(\Delta\sigma/\sigma)_{\mathrm{stat}}$ (%)
1 b-tag	11500	61000	**2.3**	**12**	**2.3**
2 b-tag	8000	20000	**1.6**	**10**	**2.0**

4 Kinematic Top-Mass Reconstruction with Fully Hadronic Events

The sample selected with the cuts described in Section 3.2, including the demand for two b-tags, represents the starting point for a kinematic top-mass reconstruction in fully hadronic events. Applying an additional cut of the form $100\ \mathrm{GeV}/c < p_\mathrm{T} < 300\ \mathrm{GeV}/c$ on the two leading jets, whose distributions are shown in Figure 19, affects the signal purity only minimally but is effective against the intrinsic backgrounds of the selected signal events. These backgrounds stem from mis-reconstructed events according to the jet-parton-matching, see Section 4.1, and from combinatorial background, described in Section 4.2.

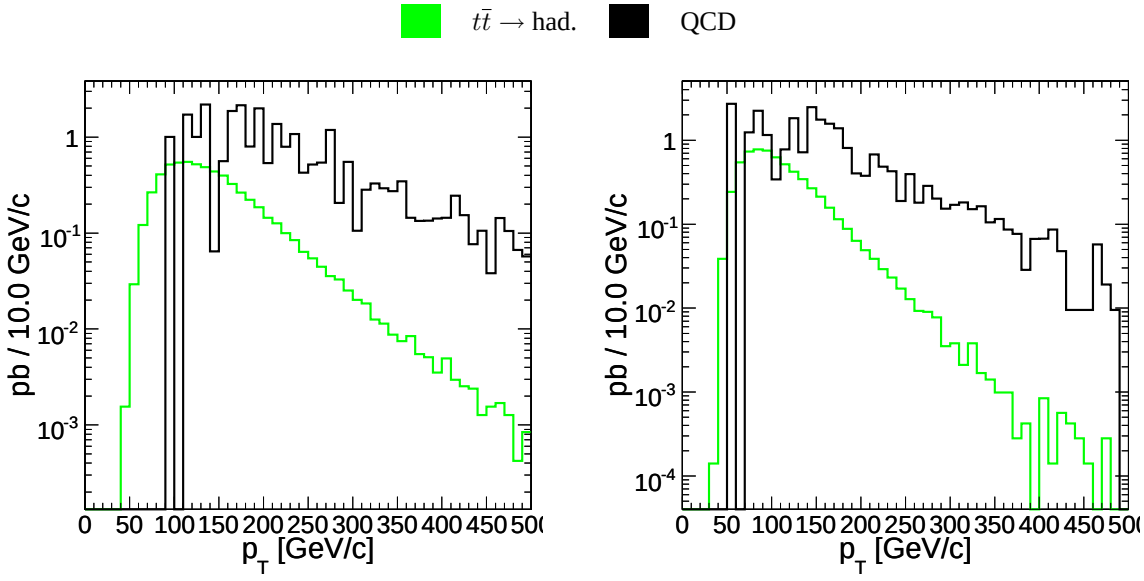

(a) (b)

Figure 19: p_T-distributions for selected signal and background events (a) for leading and (b) second-leading jet.

4.1 Jet-Parton-Matching

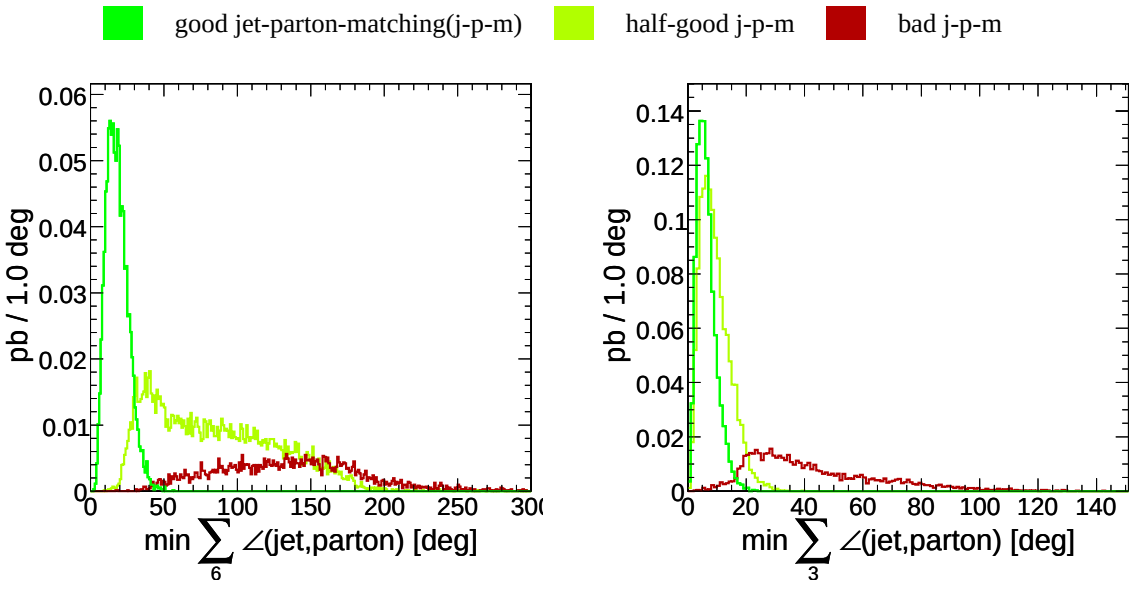

(a) (b)

Figure 20: Jet-parton-matching quality plots for the three classes of signal events discussed in the text: (a) minimal space-angle sum for both tops and (b) minimal space-angle sum for the best matched of the two tops.

The six partons in $\mathrm{pp} \rightarrow \mathrm{t\bar{t}} \rightarrow \mathrm{bW^+\bar{b}W^-} \rightarrow \mathrm{bq_1\bar{q}_1'\bar{b}q_2\bar{q}_2'}$ are matched to six reconstructed jets by picking the matching which minimises the sum of the angular separation between reconstructed jet and matched parton. Only jets satisfying our selection requirements, $p_\mathrm{T} > 30\ \mathrm{GeV}/c$ and $|\eta| < 2.4$, are taken into account in the matching

process. The resulting angular sums are shown in Figures 20(a) and 20(b), using already the following definition of three disjunct classes of signal events:

- good jet-parton-matching: Each of the six partons and jets differ only by 15° and the jet-reconstructed tops also differ only by 15° from their corresponding parton-level direction.
- half-good jet-parton-matching: Three of the partons and jets forming one top differ only by 15° and this jet-reconstructed top also differs only by 15° from his corresponding parton-level direction.
- bad jet-parton-matching: Everything else.

The value of 15° is somewhat arbitrary, but Figure 20(a) shows a distribution well below $6 \cdot 15^\circ = 90^\circ$ for the good jet-parton-matching, confirming a separate observation that usually at most one matched jet exhibits a high angular separation from its parton.

The origin of the mismatches can be traced to parton-level properties, shown in Figures 21. Badly matched jet-parton events often contain high $|\eta|(> 2.4)$ and low $p_{\mathrm{T}}(< 20\ \mathrm{GeV}/c)$ partons, see Figures 21(b) and 21(d) respectively, thus a corresponding jet falls probably outside our jet-defintion. The energy in a cone of $R = 0.2$ around a parton normalised to the energy of the parton, plotted in Figure 21(f), indicates also hard gluon radiation, which once again the fully and partially mismatched events exhibit strongly, resulting again in a difficult jet-reconstruction.

The first class, which amounts to 36% of all selected signal events, are the most sensitive to the top-mass estimation, while the second class, those with half-good matched jet-partons, will be salvaged by trying to choose the well-reconstructed top, since it represents 45% of all selected signal events.

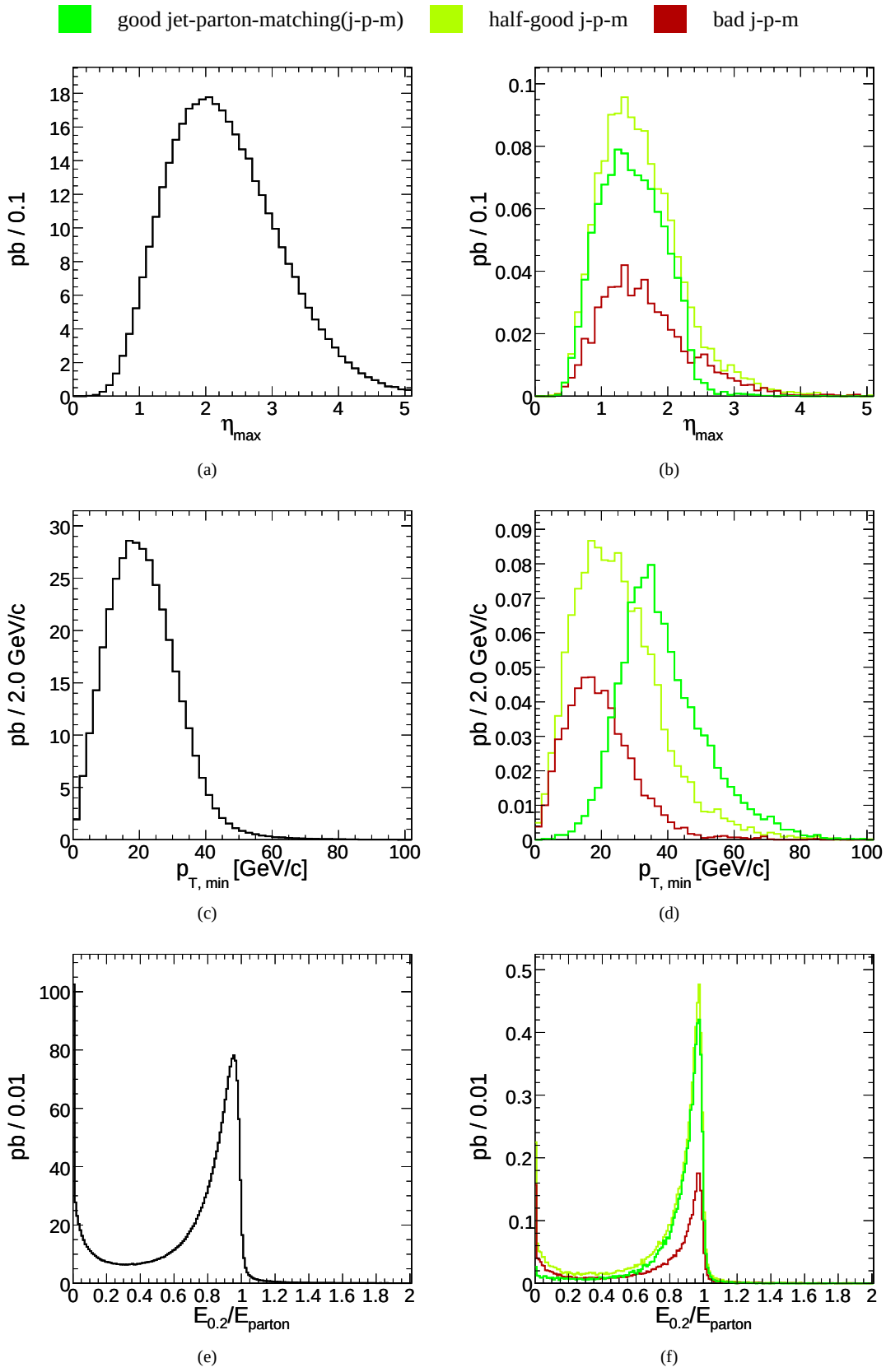

Figure 21: Parton-level properties of the six quarks in $\mathrm{pp} \to \mathrm{t\bar{t}} \to \mathrm{bW^+\bar{b}W^-} \to \mathrm{bq_1\bar{q}_1'\bar{b}q_2\bar{q}_2'}$, on the left for all hadronic $t\bar{t}$ events and on the right for the selected ones accordingly divided in the three matching classes. (a), (b): maximal $|\eta|$ of the six quarks. (c), (d): minimal p_T of the six quarks. (e), (f): energy in a cone of $R = 0.2$ around each parton normalized to the energy of the parton.

4.2 Jet-Pairing

There are 10 pairings to combine 6 jets into 2 unique top vectors, as visualised in Figure 22. On the one hand, the number of pairings decreases to 6, if both b-jets are known and used. On the other hand, the number of pairings increases by a factor of $\binom{n}{6}$ for n reconstructed jets and based on the selection $6 \leq n \leq 8$ can occur and is taken into account.

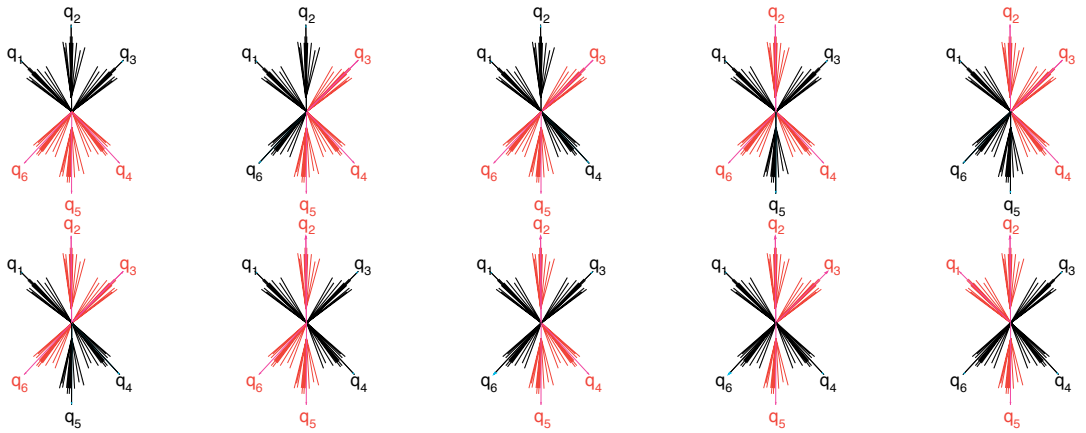

Figure 22: 10 pairings to combine 6 jets into 2 unique top vectors.

In order to perform the correct jet-pairing, a likelihood variable is constructed from the following event observables:

a) average of the W-candidates' masses

b) difference of the W-candidates' masses

c) sum of the W-candidates' jet-angles $\angle(\mathrm{q}_1\bar{\mathrm{q}}_1') + \angle(\mathrm{q}_2\bar{\mathrm{q}}_2')$

d) difference of the top-candidates' masses

e) sum of the top-candidates' jet-angles $\left(\angle(\mathrm{bq}_1) + \angle(\mathrm{b}\bar{\mathrm{q}}_1') + \angle(\mathrm{q}_1\bar{\mathrm{q}}_1')\right) + \left(\angle(\bar{\mathrm{b}}\mathrm{q}_2) + \angle(\bar{\mathrm{b}}\bar{\mathrm{q}}_2') + \angle(\mathrm{q}_2\bar{\mathrm{q}}_2')\right)$

f) angle between the top-candidates

The distributions of these inputs for the likelihood pairing function are shown in Figure 23 and are based on the selected signal events with good jet-parton-matching. The resulting likelihood variable discriminates nicely between correct and wrong pairings, as can be seen in Figure 24.

Taking for each event the pairing with the highest likelihood value results in the distribution shown in Figure 25, and after cutting on this output at a value of 0.99 one gets the pairing efficiencies detailed in Table 12. Out of the defined three reconstruction classes, the additional differentiation between correct and wrong pairing is only applicable to the good and half-good reconstructed events, resulting in five event classes.

Table 12: Distribution of the different signal event classses after imposing the pairing that gives the maximal output of the likelihood pairing function and discarding events with values smaller than 0.99.

	reconstruction	pairing	[pb]
$t\bar{t} \rightarrow$ had.	good	correct	0.62 (35%)
		wrong	0.26 (14%)
	half-good	correct	0.46 (25%)
		wrong	0.26 (15%)
	bad	always wrong	0.20 (11%)

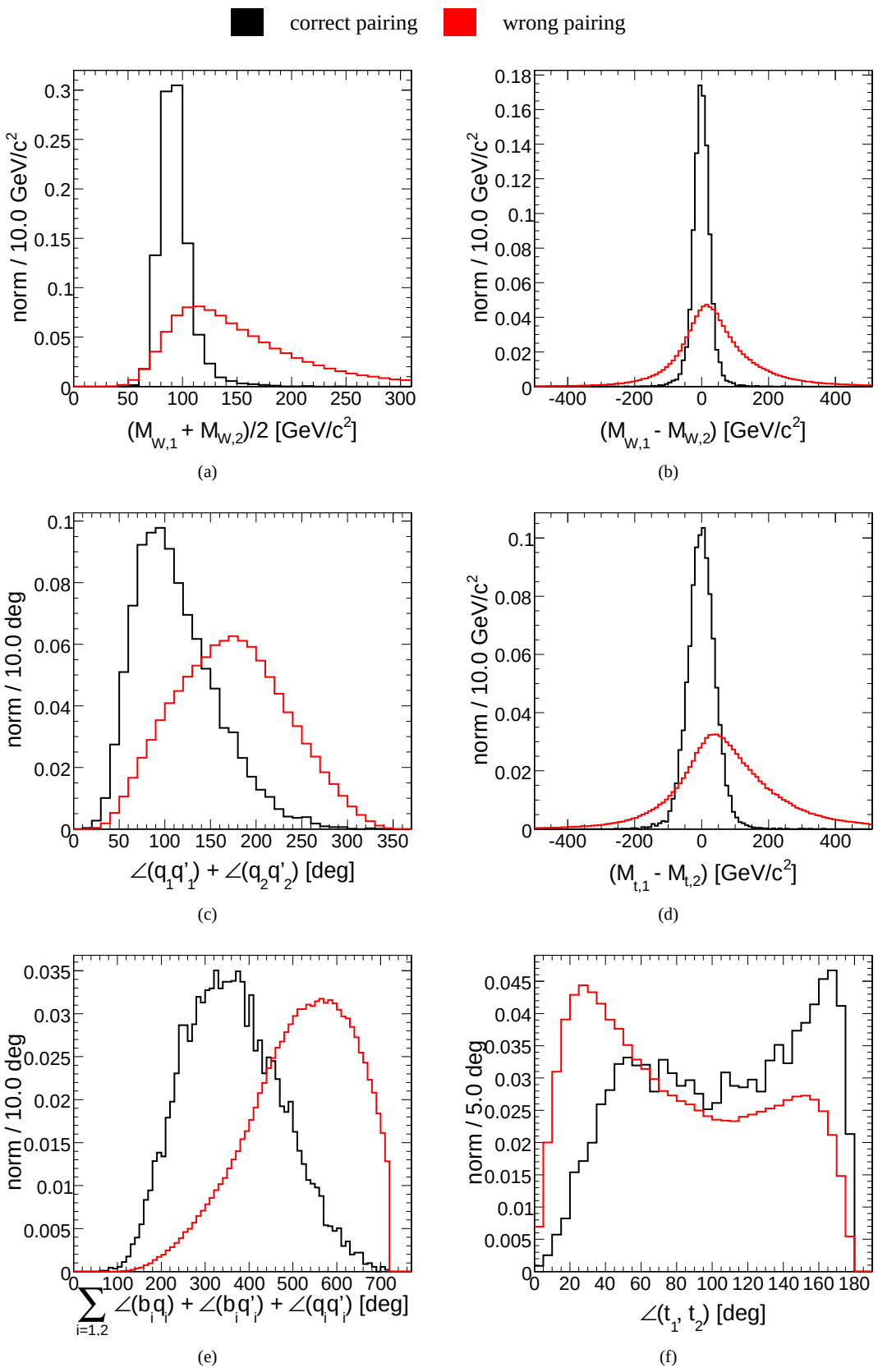

Figure 23: Inputs for the likelihood pairing function: (a) average of the W-candidates' masses, (b) difference of the W-candidates' masses, (c) sum of the W-candidates' jet-angles $\angle(\mathrm{q_1\bar{q}'_1}) + \angle(\mathrm{q_2\bar{q}'_2})$, (d) differences of the top-candidates' masses, (e) sum of the top-candidates' jet-angles $(\angle(\mathrm{bq_1}) + \angle(\mathrm{b\bar{q}'_1}) + \angle(\mathrm{q_1\bar{q}'_1})) + \left(\angle(\mathrm{\bar{b}q_2}) + \angle(\mathrm{\bar{b}\bar{q}'_2}) + \angle(\mathrm{q_2\bar{q}'_2})\right)$, (f) angle between the top-candidates.

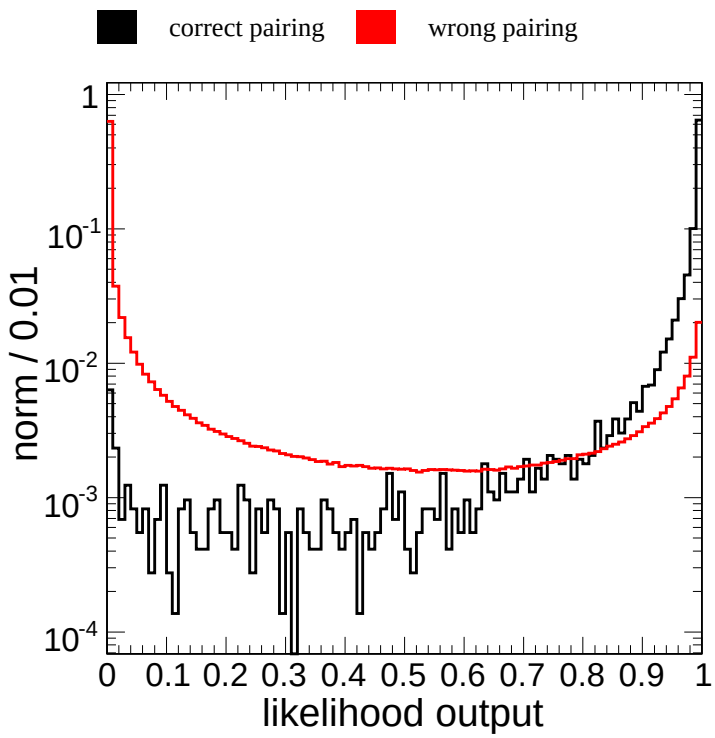

Figure 24: Output of the likelihood pairing function for all pairings.

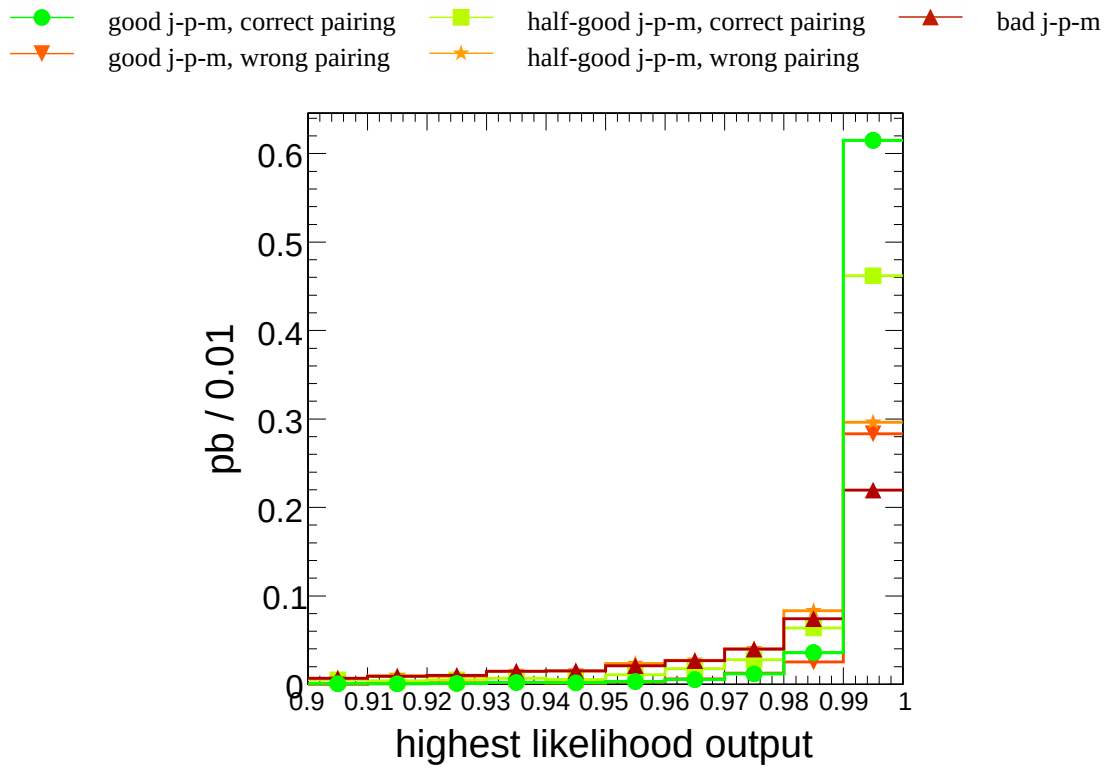

Figure 25: Maximal output value of the likelihood pairing function for all selected signal events divided into their a posteriori five event classes.

4.3 Top-Choice

In order to recover some signal from the intrinsic backgrounds of our selected hadronic $t\bar{t}$ events, only one top is chosen for the kinematic mass determination. Once again a likelihood variable is constructed, this time from the following event observables:

a) top-candidate's smallest jet-p_{T} from its constituents $\mathrm{b_i}, \mathrm{q_i}, \bar{\mathrm{q}}_\mathrm{i}'$

b) top-candidate's enclosed W-mass

c) top-candidate's jet-angles $(\angle(\mathrm{b_i q_i}) + \angle(\mathrm{b_i}\bar{\mathrm{q}}_\mathrm{i}') + \angle(\mathrm{q_i}\bar{\mathrm{q}}_\mathrm{i}'))$

The distributions of these inputs for the top-choice likelihood are shown in Figure 26 and are based on the selected signal events with half-good jet-parton-matching and correct pairing. The resulting likelihood variable discriminates decently between correct and wrong choice, as can be seen in Figure 26(d). Taking the top with the higher likelihood output yields a 72% efficiency, far greater than the 50% efficiency of a random choice.

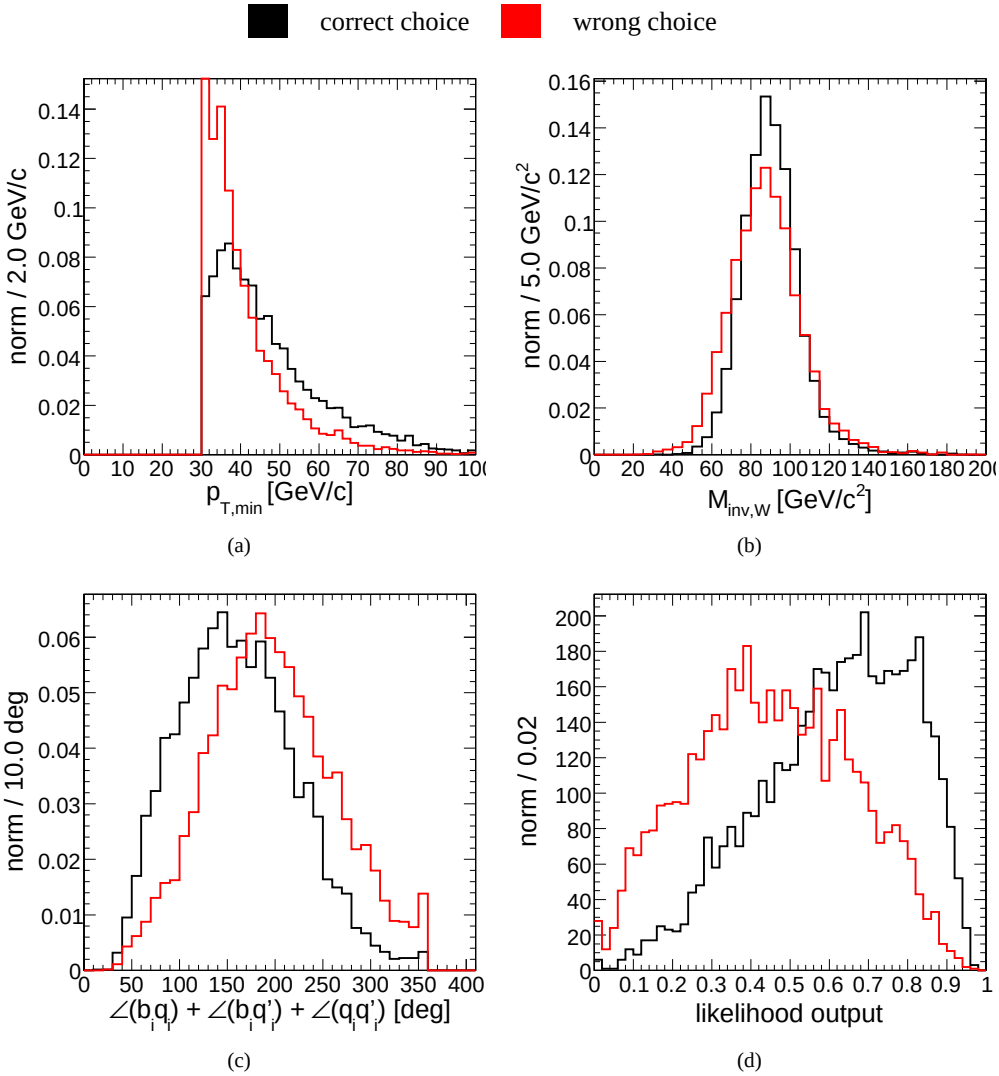

Figure 26: Input for the top-choice likelihood: (a) top-candidate's smallest jet-p_{T} from its constituents $\mathrm{b_i}, \mathrm{q_i}, \bar{\mathrm{q}}_\mathrm{i}'$, (b) top-candidate's enclosed W-mass, (c) top-candidate's jet-angles $(\angle(\mathrm{b_i q_i}) + \angle(\mathrm{b_i}\bar{\mathrm{q}}_\mathrm{i}') + \angle(\mathrm{q_i}\bar{\mathrm{q}}_\mathrm{i}'))$, resulting in the output (d).

The differentiation of the selected signal events into the now six classes is summarised in Table 13, where the six classes are being mapped onto two labels, indicating whether the events are considered signal- or background-like.

Table 13: Distribution of the different signal event classes after jet-pairing and top-choice. The label column indicates whether the class is considered signal- or background-like.

	reconstruction	pairing	[pb]	top-choice	[pb]	label
$t\bar{t} \rightarrow$ had.	good	correct	0.62 (35%)	always correct	0.62 (35%)	sig.
		wrong	0.26 (14%)	always wrong	0.26 (14%)	bkg.
	half-good	correct	0.46 (25%)	correct	0.33 (18%)	sig.
				wrong	0.13 (7%)	bkg.
		wrong	0.26 (15%)	always wrong	0.26 (15%)	bkg.
	bad	always wrong	0.20 (11%)	always correct	0.20 (11%)	bkg.

4.4 Mass Determination

With all the pieces in place a kinematic reconstruction of the top quarks is straightforward. The resulting invariant mass distribution of the chosen top, with the paired non-b-jets rescaled such that they yield the W-mass, is shown in Figure 27(c).

As expected the signal-like events form a narrow peak, while the background-like events, which still contain top-mass information, have a far broader shape. As a comparison, the distribution of the average invariant mass is shown in Figure 27(d), now with only events coloured as signal-like, where both top quarks are paired correctly. Fitting a Gaussian to the peak of the invariant mass distributions with a fit range corresponding to all bins containing more than 40% of the entries at the maximum, as shown in Figures 27(c) and 27(d), serves as a simple mass estimator. Its linearity is shown in Figures 27(e) and 27(f). The non-averaged mass distribution yields the best linearity, with a slope closer to unity. The deviation is still large enough to demand a correction factor depending on the value of the slope. The extracted top-mass is

$$m_t = 175.0 \pm 0.6\ (\text{stat.}) \pm 4.2\ (\text{syst.})\ \text{GeV}/c^2$$

for an input top-mass of $175\ \text{GeV}/c^2$ and an integrated luminosity $\mathcal{L} = 1\ \text{fb}^{-1}$, and already the statistical error becomes negligible compared to the systematic ones.

The same systematic sources described in detail in Section 2.2.4 have been considered. Their influence on the kinematic top-mass determination with fully hadronic events has been summerised in Table 14.

Table 14: Summary of the systematic uncertainties for the top-mass determination with fully hadronic events.

	$\Delta m_t[\ \text{GeV}/c^2]$
Pile Up	0.4
Underlying Event	0.6
PDF	1.4
IS/FS Radiation	2.3
Fragmentation	0.9
Jet Energy Scale	2.3
b-Tagging	0.3
Background	2.0

Most of the systematic uncertainties have been estimated according to the suggestions in reference [2]. The pile-up value is derived as the full difference between simulated samples with and without in-time pile-up for the low luminosity $\mathcal{L} = 2 \times 10^{33}\ \text{cm}^{-2}\,\text{s}^{-1}$ scenario. The jet energy scale is treated according to the functional form given in [8], estimated to be valid for the first $1 - 10\ \text{fb}^{-1}$ of data. For offline b-tagging an uncertainty of 4%(barrel)/5%(endcap) [1] has been investigated.

By far the biggest systematic uncertainty is the QCD background. The signal-to-background ratio in the displayed mass window of Figures 27(a) and 27(b) is $\sim 2/3$, the QCD background having been further suppressed by the likelihood pairing function cut and by having invariant masses above $350\ \text{GeV}/c^2$. The low number of remaining QCD events, namely 29 events, selected from the full 2.8M events of the official simulated datasets, coupled with

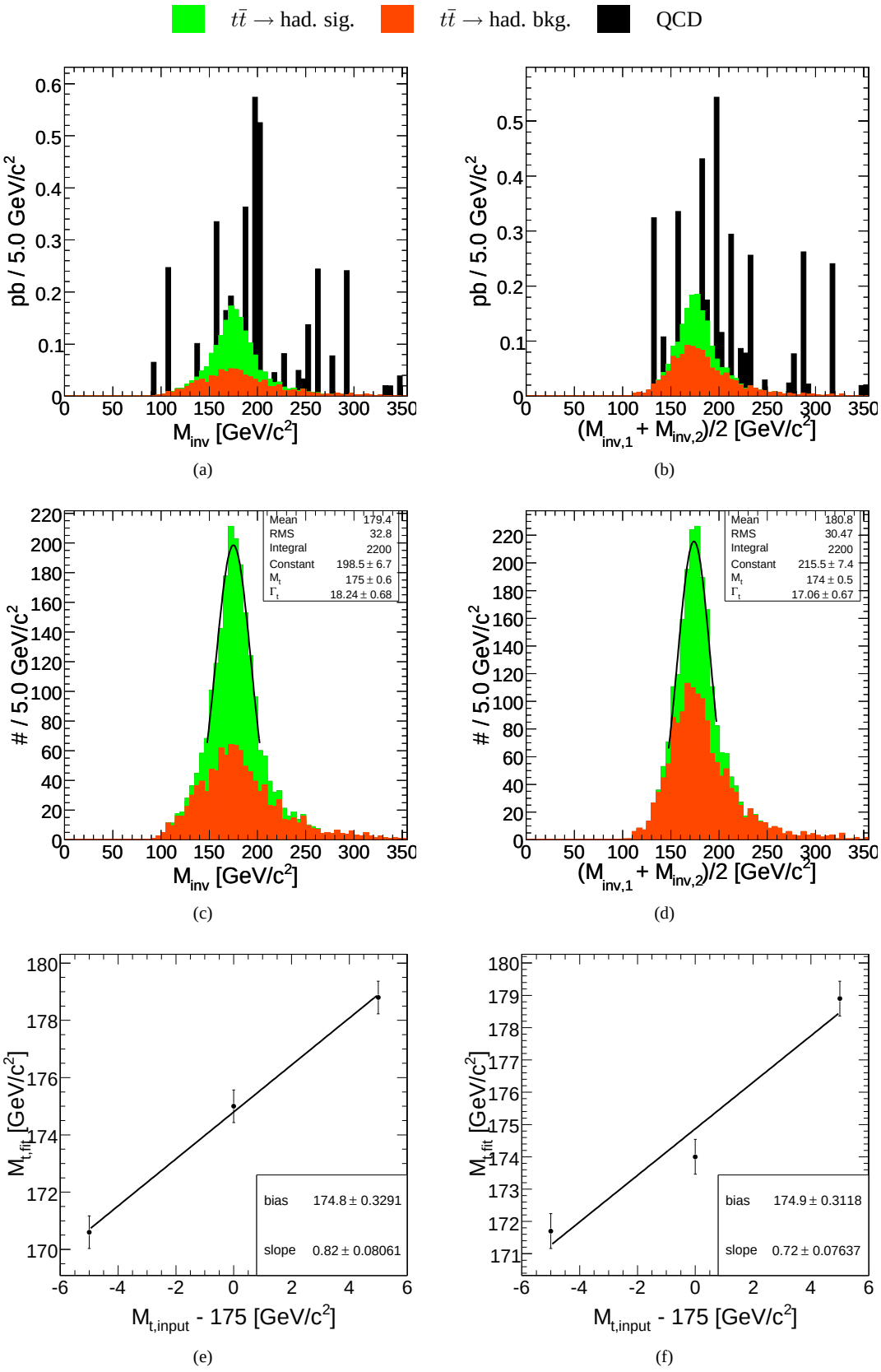

Figure 27: Invariant mass distribution of the reconstructed and rescaled top(s), on the left for the chosen top, and on the right for the average of both tops. (a), (b): for selected background and both signal classes, (c), (d): for both signal classes with Gaussian fit to the peak, (e), (f): linearity of the mass estimator.

the high cross-section scaling factors, lead to the spike structure shown in the figures, and it is hard to quantify the uncertainty at this stage. Further studies with more simluated events will be required to reveal its shape more precisely. Improved selections, like the neural network based one in section 3.4, or even completely mass-specific selections should be able to further suppress the QCD background. Experience from CDF at the Tevatron [10, 11] indicates that this uncertainty can be understood at the $\sim 2\ \mathrm{GeV}/c^2$ level, when using data for background estimation.

5 Summary and Conclusion

The selection of $t\bar{t}$ events with the CMS experiment at the LHC has been presented. In the $t\bar{t}$ decay modes considered here, di-lepton, and fully hadronic, the signal can be established with high significance, allowing to measure the $t\bar{t}$ production cross section precisely. The selected event samples allow an accurate determination of the mass of the top quark and set the stage for precision determinations of its other properties.

6 Acknowledgements

We would like to thank our CMS colleagues, especially Martijn Mulders, Christian Weiser and Juan Alcaraz, for valuable discussions.

References

[1] C. Weiser. A Combined Secondary Vertex Based B-Tagging Algorithm in CMS. *CMS Note*, 2006/014, 2006.

[2] P. Bartalini, R. Chierici, and A. De Roeck. Guidelines for the Estimation of Theoretical Uncertainties at the LHC. *CMS Note*, 2005-013, 2005.

[3] CMS Collaboration. CMS Physics TDR Volume 1. *CERN/LHCC*, 2006-001, 2006.

[4] S. Gennai et al. Tau jet reconstruction and tagging at High Level Trigger and off-line. *CMS Note*, 2006/028, 2006.

[5] CMS Collaboration. The TriDAS Project Technical Design Report, Volume 2: Data Acquisition and High-Level Trigger. *CERN/LHCC*, 2002-26, 2002. CMS TDR 6.2.

[6] M. Vos and F. Palla. B-tagging in the High Level Trigger. *CMS Note*, 2006/030, 2006.

[7] CDF Collaboration and D0 Collaboration (Daniel Wicke for the collaboration). Top Pair production cross-section measurement in the all-hadronic channel at CDF and D0. *Int. J. Mod. Phys. A*, 20:3183–3186, 2005.

[8] A. et al. Heister. Measurement of Jets with the CMS Detector at the LHC, 2006. CMS Note 2006/036.

[9] R. Brun and F. Rademakers. ROOT - An Object Oriented Data Analysis Framework. In *AIHENP'96 Workshop*, volume Phys. Res. A 389, pages 81–86, Lausanne, Switzerland, September, 1996 1997.

[10] Abe, F. and others. First observation of the all hadronic decay of t anti-t pairs. *Phys. Rev. Lett.*, 79:1992–1997, 1997.

[11] Group, Tevatron Electroweak Working. Combination of CDF and D0 results on the mass of the top quark. 2006.